J Physiol 588.24 (2010) pp 4995–5014

The Journal of Physiology

Hydrogen ion dynamics in human red blood cells

Pawel Swietach[1], Teresa Tiffert[2], Jakob M. A. Mauritz[2,3], Rachel Seear[2], Alessandro Esposito[2,3], Clemens F. Kaminski[3], Virgilio L. Lew[2] and Richard D. Vaughan-Jones[1]

[1]*Department of Physiology, Anatomy and Genetics, Burdon Sanderson Cardiac Science Centre, Parks Road, Oxford OX1 3PT, UK*
[2]*Physiological Laboratory, Department of Physiology, Development and Neuroscience, University of Cambridge, Cambridge CB2 3EG, UK*
[3]*Department of Chemical Engineering and Biotechnology, University of Cambridge, Cambridge CB2 3RA, UK*

Our understanding of pH regulation within red blood cells (RBCs) has been inferred mainly from indirect experiments rather than from *in situ* measurements of intracellular pH (pH_i). The present work shows that carboxy-SNARF-1, a pH fluorophore, when used with confocal imaging or flow cytometry, reliably reports pH_i in individual, human RBCs, provided intracellular fluorescence is calibrated using a 'null-point' procedure. Mean pH_i was 7.25 in CO_2/HCO_3^--buffered medium and 7.15 in Hepes-buffered medium, and varied linearly with extracellular pH (slope of 0.77). Intrinsic (non-CO_2/HCO_3^--dependent) buffering power, estimated in the intact cell (85 mmol (l cell)$^{-1}$ (pH unit)$^{-1}$ at resting pH_i), was somewhat higher than previous estimates from cell lysates (50–70 mmol (l cell)$^{-1}$ (pH unit)$^{-1}$). Acute displacement of pH_i (superfusion of weak acids/bases) triggered rapid pH_i recovery. This was mediated via membrane Cl^-/HCO_3^- exchange (the AE1 gene product), irrespective of whether recovery was from an intracellular acid or base load, and with no evident contribution from other transporters such as Na^+/H^+ exchange. H^+-equivalent flux through AE1 was a linear function of $[H^+]_i$ and reversed at resting pH_i, indicating that its activity is not allosterically regulated by pH_i, in contrast to other AE isoforms. By simultaneously monitoring pH_i and markers of cell volume, a functional link between membrane ion transport, volume and pH_i was demonstrated. RBC pH_i is therefore tightly regulated via AE1 activity, but modulated during changes of cell volume. A comparable volume–pH_i link may also be important in other cell types expressing anion exchangers. Direct measurement of pH_i should be useful in future investigations of RBC physiology and pathology.

(Received 4 August 2010; accepted after revision 18 October 2010; first published online 20 October 2010)
Corresponding author P. Swietach: Department of Physiology, Anatomy and Genetics, Burdon Sanderson Cardiac Science Centre, Parks Road, Oxford OX1 3PT, UK. Email: pawel.swietach@dpag.ox.ac.uk

Abbreviations CA, carbonic anhydrase; RBC, red blood cell.

Introduction

Red blood cells (RBCs) play a fundamental role in regulating the acid–base balance of extracellular fluids. Two key molecular elements for this in the RBC are haemoglobin (Hb) and the AE1 isoform of the anion-exchange transporter (also referred to as Band 3). Haemoglobin, at a concentration of 7 mmoles per litre of cell water (mmol (l cell water)$^{-1}$), is the RBC's main proton (H^+ ion) buffer (Cass & Dalmark, 1973). AE1, expressed with over 10^6 copies per human RBC (Alper, 1991), mediates a rapid transmembrane exchange of Cl^- for HCO_3^-, thereby enhancing the mass transport of CO_2 in the form of plasma HCO_3^-. AE1 activity is facilitated by cytoplasmic carbonic anhydrase (CA), an enzyme that catalyses the reversible hydration of carbon dioxide ($CO_2 + H_2O \rightleftharpoons HCO_3^- + H^+$) (Meldrum & Roughton, 1933; Maren, 1967). Efficient AE1 activity in the RBC is critical for lung clearance of metabolically produced CO_2, and thus for the maintenance of plasma and whole-body pH.

While the role of RBCs in the regulation of plasma pH has been studied extensively (Van Slyke *et al.* 1923; Funder & Wieth, 1966), much less is known about hydrogen ion dynamics within the RBCs themselves. The control of RBC pH_i has usually been inferred from pH measurements after cell lysis (Cass & Dalmark, 1973), from changes of extracellular pH (pH_o) during RBC activity (Freeman *et al.* 1987), from radiotracer measurements of Cl^- flux (Funder & Wieth, 1976), and from mathematical model predictions (Lew & Bookchin, 1986; Lew *et al.* 1991). Direct pH_i recordings, however,

DOI: 10.1113/jphysiol.2010.197392

have rarely been made. Progress in the field has been hindered by difficulties associated with monitoring intracellular ion concentrations in the intact RBC. The cells are too fragile and small to support stable impalement by ion-sensitive micropipettes. Furthermore, the use of some types of intracellular ion-sensitive fluorophore is frustrated by fluorescence quenching from intracellular Hb (Lew *et al.* 1993). A previous report has described the use of the pH fluorophore, BCECF, for recording average pH_i in a population of RBCs (several million) suspended in solution within a cuvette (Kummerow *et al.* 2000). The method, however, was not validated for pH_i measurement in individual cells, and the extracellular milieu was not controlled by continuous superfusion. In addition, BCECF has been shown to inhibit the RBC Ca^{2+}-ATPase (Gatto & Milanick, 1993), which may have a secondary impact on pH_i and volume homeostasis.

In the present work, the potential problems of directly recording RBC pH_i have been overcome with the use of the ratiometric pH indicator SNARF-1 (carboxy-seminaphthorhodafluor-1), diffused as the acetoxymethyl (AM) ester into the cell (Buckler & Vaughan-Jones, 1990). The dye appears not to affect RBC Ca^{2+}-ATPase activity, and it provides a signal sufficient for recording pH_i in *individual* cells, despite the presence of Hb. Although difficulties were encountered with calibrating the signal using a classical 'nigericin' method (as also reported for renal mesangial cells; Boyarsky *et al.* 1996), an alternative, null-point method proved effective. Measurement of intracellular SNARF-1 fluorescence was combined with confocal imaging or flow cytometry, in order to characterise the control of pH_i in the RBC, and its sensitivity to pH_o. The work highlights major roles for intracellular Hb and plasmalemmal AE1. Of particular interest is pH_i regulation in the presence of physiological levels of CO_2/HCO_3^-, as the majority of previous work on H^+-equivalent transport in the RBC has been performed in the nominal absence of this physiological buffer.

In addition to investigating pH_i regulation, its role during changes of cell volume has also been explored. Direct measurements of pH_i have been used to test key predictions of a mathematical model of RBC volume homeostasis (Lew & Bookchin, 1986; Lew *et al.* 1991). The model predicts that changes of pH_o will modulate cell volume and pH_i by influencing the activity of AE1. Similarly, RBC dehydration, induced by the opening of Ca^{2+}-activated KCNN4 (KCa3.1) channels in the plasmalemma, is predicted to cause a pH_i change, again through recruitment of AE1 activity. This latter volume–pH_i link has been suggested to occur in clinical episodes of sickle-cell anaemia (Bookchin *et al.* 1991; Lew & Bookchin, 2005), an inherited disease associated with the polymerisation of mutant haemoglobin (Hb S), leading to RBC dehydration. Activity of AE1 in the RBC is thus closely integrated into the mechanism of cell volume homeostasis. In the present work, simultaneous pH_i and volume measurements have been made for individual RBCs, using confocal imaging and flow cytometry. Volume–pH_i coupling has been assessed by manipulating pH_o or activating KCNN4 membrane channels (Gardos, 1958; Vandorpe *et al.* 1998; Begenisich *et al.* 2004). The results provide the first direct validation of pH_i signalling during RBC volume regulation, and emphasise a key role for AE1.

Methods

Solutions and chemicals

The main solutions used were (in mM): 'solution A': NaCl, 142; KCl, 3; Hepes, 10; and $MgCl_2$, 0.15; 'solution B': NaCl, 132; NaSCN, 10; KCl, 3; Hepes, 10; and $MgCl_2$, 0.15; 'solution C': NaCl, 42; NaSCN, 10; KCl, 90; Hepes, 10; and $MgCl_2$, 0.15. For superfusion experiments, solution pH was adjusted to 7.4 at 37°C. For flow cytometry experiments, solution pH was adjusted to 7.4 (unless stated otherwise) at 25°C. Some superfusion experiments were performed in the presence of physiological CO_2/HCO_3^- buffer, instead of Hepes. For these, solutions were modified to include 22 mM $NaHCO_3$ (replacing 22 mM NaCl) and bubbled with 5% CO_2 (balanced with air) at 37°C to equilibrate at a pH of 7.4. All solutions were in equilibrium with atmospheric O_2 partial pressure.

Where noted, additions were as follows (final concentrations in the cell suspension or in superfusate, in mM): NaOH-neutralized EGTA, 0.1; $CaCl_2$, 0.25; NH_4Cl, 30 (replacing 30 mM NaCl); sodium acetate, 80 (replacing 80 mM NaCl); sodium gluconate, 100 (replacing 100 mM NaCl); inosine, 5; pyruvate, 5; ionomycin (from 10 mM stock in DMSO), 0.01; acetoxymethyl (AM) ester of SNARF-1 (SNARF-1-AM), 0.01; NS309 (6,7-dichloro-1*H*-indole-2,3-dione 3-oxime; from 10 mM stock in DMSO; Strobaek *et al.* 2004), 0.01; nigericin, 0.01 μM; 4,4′-diisothiocyanato-stilbene-2,2′-disulfonate (DIDS), 0.3 (Cabantchik & Rothstein, 1972).

SCN^- was used to by-pass the rate-limiting effects of anion permeation on the speed of dehydration of RBCs with upregulated K^+ conductance. Ten millimolar SCN^- was sufficient to saturate this effect (Garcia-Sancho & Lew, 1988). Inosine was used as glycolytic substrate and pyruvate was added to bypass the glycolytic block imposed by the release of formaldehyde during the de-esterification of SNARF-1-AM (Tiffert *et al.* 1984; Garcia-Sancho, 1985). All chemicals were analytical reagent quality. NaSCN, sodium gluconate, EGTA, Hepes, DMSO, inosine, pyruvate, NS309, nigericin and ionomycin were from Sigma-Aldrich (Poole, UK). SNARF-1-AM was from Invitrogen (Paisley, UK). $CaCl_2$, $MgCl_2$, NaCl and KCl were from FSA Laboratory Supplies (Loughborough, UK).

Preparation of RBCs

After obtaining informed written consent, venous blood from healthy volunteers was drawn into tubes containing EDTA (ethylenediaminetetraacetic acid) to reduce plasma Ca^{2+} concentration and prevent clotting, washed twice in solution A with added EGTA, and twice more with solution A. The buffy coat (platelets and white cells) was removed after each wash. The washed RBCs were suspended at 0.1–1% haematocrit (Hct) in solution A, supplemented with inosine, pyruvate and SNARF-1-AM (10 μM) and incubated for 5 min at 37°C to allow for de-esterification and trapping of SNARF-1 inside RBCs.

RBC volume (measured using flow cytometry) followed for up to 40 min in solution A supplemented with 0.25 mM $CaCl_2$, was not affected by SNARF-1 loading. This is relevant because if SNARF-1 had significant inhibitory effects on the plasma membrane Ca^{2+} pump, as claimed for the pH fluorophore BCECF (Gatto & Milanick, 1993), the cells would load with Ca^{2+}, leading to dehydration and cell shrinkage (Lew & Bookchin, 1986). Figure S1 in the online Supplemental Material illustrates that exposure to 1 or 5 mM vanadate, a plasma membrane Ca^{2+} pump inhibitor, caused cell dehydration, while AM-loading of SNARF-1 (10 μM) over the same time period (35 min) exerted no effect. SNARF-1 thus appears to exert little or no inhibitory effect on RBC Ca^{2+} homeostasis.

Superfusion and confocal fluorescence imaging

Superfusion was performed in a 2 ml Perspex chamber with a coverslip base, mounted on an inverted Leica IRBE microscope. A volume of 150 μl of the suspension with SNARF-1 loaded cells was carefully pipetted onto the coverslip, and the cells left to settle for about 10 min at room temperature. Cells were subsequently superfused with solution at 37°C, delivered at 2 ml min^{-1}, to wash away extracellular SNARF-1 and any cells that had not settled on the coverslip surface.

Intracellular SNARF-1 was imaged confocally using a Leica TCS NT system. An argon laser excited the dye at 514 nm and fluorescence emission was collected at 580 nm and 640 nm simultaneously (with 40 nm band-pass filters) in *xy* scanning mode at a pixel resolution of 256 × 256 once every 1.1 s. To maximise emission signal, the pinhole was set to 2 Airy units. Fluorescence intensity at the two wavelengths was ratioed and converted to pH using a calibration curve.

Flow cytometry

A minimum of 150 μl of suspension with SNARF-1 loaded cells was aspirated through a flow cytometer (Quanta SC, Beckman Coulter, Brea, CA, USA). The intracellular dye was excited with a 488 nm laser and emission was collected at 630 nm and 575 nm through 30 nm band-pass filters. The ratio of fluorescence intensities at the two wavelengths was converted to pH using a calibration curve. Cell volume was measured simultaneously and independently of fluorescence. Volume calibration was performed using 10 μm-diameter spheres (Beckman Coulter). Due to limitations imposed by the equipment, measurements were performed at room temperature (25°C).

Experimental protocols

***In situ* calibration of the SNARF-1 fluorescence ratio using nigericin.** Cells were superfused at 37°C (for confocal imaging) or suspended at 25°C (for flow cytometry) with high-K^+ medium adjusted to different levels of pH within the range 5.5 to 9.5 by addition of HCl or NaOH from 5 M stocks. Two sets of calibration solutions were used for the 'nigericin method'. The first set (140-K) contained (in mM): NaCl, 5; KCl, 140; $MgCl_2$, 0.15; Hepes (for the pH range 6.6–8.1) or Mes (for pH 5.5–6.6) or Hepps (for pH 8.1–9.5), 10. The second set (100-K) was a modification of the above, containing 100 mM KCl and 45 mM NaCl. All solutions also contained the K^+/H^+ ionophore nigericin (10 μM). After allowing at least 2 min for equilibration, the SNARF-1 fluorescence ratio was plotted against solution pH to obtain a calibration curve (Thomas *et al.* 1979). The accuracy of the nigericin method relies on careful matching of intracellular K^+ with extracellular K^+ (Boyarsky *et al.* 1996), and therefore two sets of calibration solutions of different $[K^+]$ were used to encompass the possible range of $[K^+]$ inside RBCs.

***In situ* calibration of the SNARF-1 fluorescence ratio using the null-point technique.** RBCs under confocal imaging were superfused with isosmotic solutions at 37°C containing a mixture of salts of a weak base (ammonium chloride) and weak acid (sodium acetate). For flow cytometry, cells were suspended at 25°C in similar solutions for 2–5 min before pH_i measurements were made. The $[NH_4^+]$/[acetate] ratio was varied in the different solutions (see Appendix for equations relating to the null-point method). At the 'null-point pH' (pH_{null}), exposure of an RBC to a particular ratio will produce no overall pH_i change, as the deprotonation of acetic acid within the cell is offset by the protonation of intracellular NH_3 (Eisner *et al.* 1989; Buckler & Vaughan-Jones, 1990). The null-point solutions at 37°C had the following concentrations of NH_4Cl and sodium acetate (in mM): 'pH 7.5': 5, 3.08; 'pH 7.4': 5, 4.9; 'pH 7.3': 5, 7.75; 'pH 7.2': 5, 12.28; 'pH 7.1': 5, 19.45; 'pH 7.0': 2, 12.33; 'pH 6.9': 2, 19.55; 'pH 6.8': 2, 31; 'pH 6.7': 2, 49.1. The null-point solutions at 25°C had the following concentrations of NH_4Cl and sodium acetate (in mM): 'pH 7.3': 5, 7.83; 'pH 7.2': 5, 12.41; 'pH 7.1': 5, 19.67; 'pH 7.0': 5, 31.18. These

calculations have assumed a pK for NH_4^+ and acetic acid of 9.03 and 4.528 at 37°C, and 9.25 and 4.75 at 25°C. The null-point method assumes that the weak acid/base enters cells principally in the uncharged form. To block any possible entry of acetate or ammonium ions via anion exchange and K^+ channels, respectively, all null-point solutions contained DIDS (300 μM) and Ba^{2+} (1 mM) (Leem *et al.* 1999). The Appendix provides further details of the assumptions and equations used in the null-point technique.

Measurement of RBC hydrogen ion buffering capacity. Individual RBCs were superfused with solution A in the presence of DIDS (300 μM), followed by solutions containing NH_4Cl (30, 15, 5, 0 mM; replacing NaCl isosmotically) for at least 2 min each. The fall of pH_i (ΔpH_i) on $[NH_4^+]_o$ reduction was imaged confocally, and the Henderson–Hasselbalch equation was used to estimate the fall of intracellular $[NH_4^+]$ (equal to the concentration of H^+ ions released into the cell, ΔC_H), assuming that the pK of NH_4Cl in cytoplasm is the same as in the extracellular solution. Intracellular buffering power (β) was estimated as: $\beta = -\Delta C_H/\Delta pH_i = \Delta[NH_4^+]_i/\Delta pH_i$ (Boyarsky *et al.* 1988). This value was referenced to the mid-point of the fall of pH_i on $[NH_4^+]_o$ reduction.

Tests of model predictions. Our current understanding of red blood cell homeostasis is encoded in the mathematical model of Lew & Bookchin (1986). The model includes a non-allosteric formulation for AE1, represented as an H^+–Cl^- co-transporter, with first order kinetics for transported substrates. Using this formulation to describe pH_i regulation in the RBC is justified as (i) intracellular CO_2/HCO_3^- buffering is kept close to equilibrium by high intracellular CA activity, (ii) there is a high membrane CO_2 permeability, and (iii) in imaging experiments, fast superfusion of solutions maintains extracellular CO_2/HCO_3^- buffering at equilibrium. As a result, the effect on pH_i of HCO_3^- transport is equivalent to the counter-transport of H^+. For example, imported HCO_3^- ions combine with intracellular H^+ ions, generating CO_2 (that vents across the cell membrane). This raises pH_i, which is equivalent to an efflux of H^+ ions. In the present work, predicted changes in cell pH under different experimental conditions were experimentally tested, for the first time, by making direct pH_i measurements in individual SNARF-1-loaded RBCs.

Results

Calibration of intracellular SNARF-1 fluorescence

Individual RBCs were superfused with high-K^+ (140 mM) nigericin-containing solutions adjusted to a range of pH values (Thomas *et al.* 1979). As shown in the left panel of Fig. 1*A*, the intracellular SNARF-1 emission ratio responded dynamically to changes in pH_o. This method of *in situ* dye calibration relies on the capacity of nigericin to equalise pH_i with pH_o, provided $[K^+]_o$ is set to equal $[K^+]_i$. As $[K^+]_i$ is known to fall with RBC age (Lew *et al.* 2007), the calibration procedure was repeated with RBCs superfused with 100 mM $[K^+]_o$ media (right hand panel of Fig. 1*A*), in order to bracket the likely $[K^+]_i$ range (100–140 mM). The averaged pH sensitivity of the fluorescence ratio is plotted in Fig. 1*C* for both 100 mM (filled grey circles) and 140 mM $[K^+]_o$ (open circles). The two sets of results are virtually identical.

The calibrations shown in Fig. 1*A* suggest that resting RBC pH_i was about 7.4 (ratio = 0.8), similar to the pH of normal Hepes-buffered superfusate. This value is about 0.2 units more alkaline than previous indirect estimates of RBC pH_i, and is higher than predictions based on the transmembrane $[Cl^-]$ gradient ($[Cl^-]_o > [Cl^-]_i$ therefore $[H^+]_i > [H^+]_o$; Jacobs & Stewart, 1947; Salenius, 1957; Salminen & Manninen, 1966; Dalmark, 1975), suggesting a nigericin-based calibration error. The calibration was therefore crossed-checked using a 'null-point' technique (Eisner *et al.* 1989; Boyarsky *et al.* 1996).

Salts of a membrane-permeant weak acid and base (sodium acetate and ammonium chloride) were added simultaneously to the extracellular superfusate (at a pH_o of 7.4), and a combination of concentrations was found that exerted the smallest effect on steady-state pH_i. This 'null' combination allows one to deduce the value of steady-state pH_i. The technique does not require nigericin and therefore does not rely on accurately matching $[K^+]_i$ with $[K^+]_o$. It assumes that only the uncharged species of weak acid or base is permeant, and therefore transmembrane fluxes of the charged species, acetate and NH_4^+, were minimised by including DIDS and Ba^{2+}, respectively, in solutions.

Figure 1*Ba* shows a sample time course for a null-point determination, performed on an RBC superfused with nominally CO_2/HCO_3^--free solution (Hepes buffered). The transient alkaline displacements of pH_i are due to the higher membrane permeability of ammonia, compared to acetic acid. Steady-state pH_i is, however, determined by the equilibrium concentration of weak acid and base, and independent of the relationship between ammonia and acetic acid permeability constants (see Appendix for the derivation). The weak acid/base combination for a pH_{null} of 7.1 produced the smallest steady-state displacement of the SNARF-1 emission ratio, indicating that resting pH_i was near 7.1, close to the expected value for RBCs. This is quantified further in Fig. 1*Bb*, which plots the steady-state ratio displacement, for the four null-point solutions used. By interpolation, the pH_i at which the ratio is expected to remain unchanged (the true null-point, equal to resting pH_i) was 7.13.

Best-fitting the nigericin calibration data (Grynkiewicz *et al.* 1985) indicated an apparent pK_{SNARF} for the intracellular ratio of 7.26 (Fig. 1*C*). In contrast the null-point data, averaged for several cells, yielded an intracellular pK_{SNARF} that was acid-shifted by 0.18 units (see inset to Fig. 1*C*). A typical resting RBC pH_i, derived from the null-point method, will thus be significantly lower than that from the nigericin method. Moreover, the lower value (see next section) is consistent with previous, indirect estimates of pH_i. A combined approach to *in situ* SNARF-1 calibration was also undertaken for RBC experiments using flow cytometry rather than confocal imaging (i.e. nigericin and null-point calibrations were compared). The results, shown in Supplemental Fig. S2, indicate a similar discrepancy of ∼0.2 pH_i units between the two methods, again suggesting inadequacy in the nigericin method, as applied to RBCs.

In most other cell types where *in situ* nigericin and null-point calibrations of intracellular pH fluorophore signals have been compared, the resulting pH_i values have been virtually identical (see Discussion). This is also true for a range of cultured cell lines (gift from Prof Adrian L. Harris, Oxford, UK), as reported in Supplement Fig. S3. In the isolated renal mesangial cell, however, an error of up to 0.2 pH units, comparable to that seen in RBCs, has been reported for nigericin but not for null-point calibrations (Boyarsky *et al.* 1996). Because the nigericin-based pH_i estimates could not be reconciled with the well documented equality of Cl^- and H^+ concentration ratios across RBC membranes, the null-point calibration was applied to estimate pH_i in all subsequent work reported in this paper.

Resting intracellular pH and its dependence on extracellular pH

Figure 2*A* shows the frequency distribution of resting pH_i (at pH_o 7.40), determined from confocal imaging of individual RBCs. In Hepes-buffered medium, mean pH_i was 7.15, with a coefficient of variation (C.V.) of 1.01% (mean and C.V. determined from the best-fit normal distribution). In 5% CO_2/HCO_3^- buffered medium, mean pH_i was 7.25 (C.V. = 0.99%), a slightly more alkaline value.

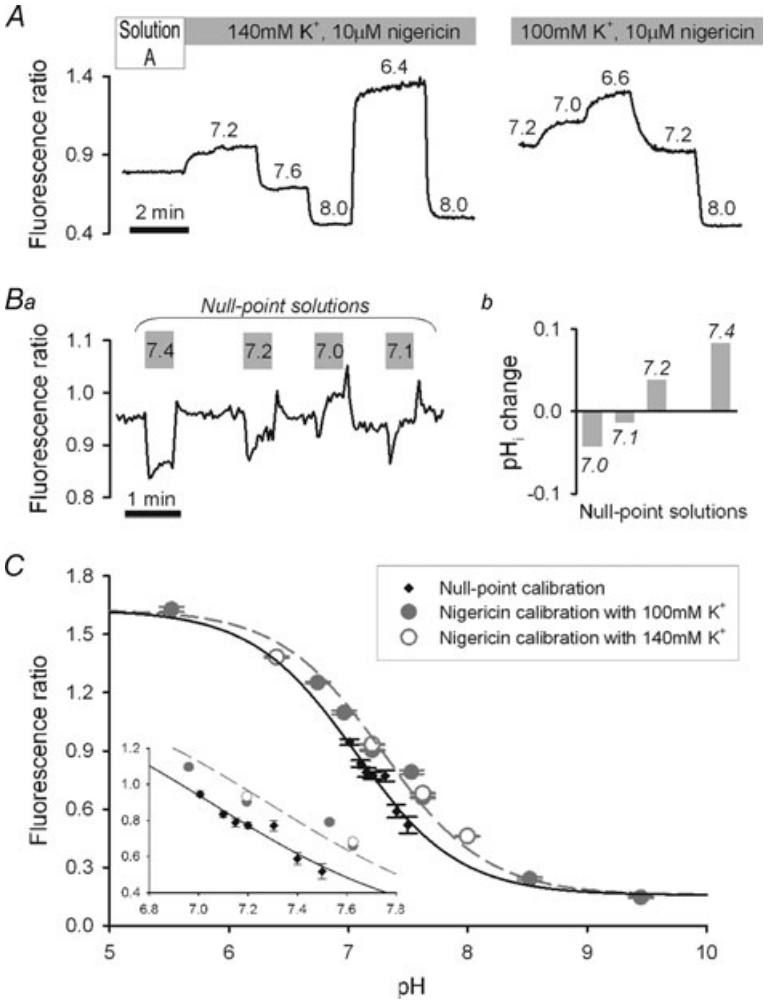

Figure 1. Calibrating intracellular SNARF-1 fluorescence ratio
A, nigericin method. Recording from a red blood cell (AM-loaded with SNARF-1) superfused with solutions containing 100 or 140 mM K^+, 300 μM DIDS and 10 μM nigericin (a K^+/H^+ ionophore). The time course shown, recorded from an individual cell, demonstrates the good fluorescence yield and pH sensitivity of the dye, in response to changes in superfusate pH_o. The Experiment shown reports a resting pH_i of ∼7.4. *B*, null-point calibration. (*a*), specimen recording from an individual red blood cell, superfused with a series of 'null-point' solutions. Exposure to a null-point solution that coincides with resting pH_i produces no net change in fluorescence ratio at the steady-state. (*b*), resting pH_i is nearest to 7.1. *C*, the data for the nigericin calibration (assuming $pH_i = pH_o$) with either 100 mM K^+ (grey filled circles; each an average of >20 cells) or 140 mM K^+ (grey open circles; each an average of >20 cells) and the null-point calibration (black circles; each an average of >5 cells). The null-point calibration is ∼0.2 units acid-shifted relative to the nigericin data, but produces a more realistic measure of resting pH_i. The nigericin calibration curve was best-fitted to a three-parameter sigmoid (dashed grey line) to estimate maximum and minimum ratio ($R_{max} = 1.595$, $R_{min} = 0.183$) and pK_{SNARF} (7.262). The null-point data were best-fitted for pK_{SNARF} (7.078; black line) using R_{max} and R_{min} obtained from the nigericin curve. The inset shows a close-up of the data near pK_{SNARF}, showing the acid-shift of the corrected calibration curve.

Resting pH_i in Hepes-buffered medium was analysed further by flow cytometry. SNARF-1 fluorescence was measured in RBCs pre-equilibrated in solutions of different pH (6.6, 7.05, 7.4 and 7.7 at 25°C). The frequency distribution of RBC pH_i in each of the four solutions was approximately normal (Fig. 2*Ba*). Mean steady-state pH_i is plotted as a function of pH_o in Fig. 2*Bb*. The relationship is linear, with a slope of 0.77 pH_i/pH_o unit. A fall of pH_o thus induces a fall of pH_i of nearly the same magnitude. The dashed line (slope $= +0.86$ pH_i/pH_o) plots the RBC model prediction for the pH_i–pH_o relationship, which is based upon the assumption that AE1 carries net H^+-equivalent fluxes until reaching equilibrium ($[Cl^-]_o/[Cl^-]_i = [H^+]_i/[H^+]_o$). The experimental measurements are in good agreement with the model predictions. The change of pH_i with pH_o is predicted, in the model, to be mediated by transmembrane H^+-equivalent flux through AE1. This was confirmed experimentally by applying the AE1 inhibitor DIDS before imposing pH_o changes, which eliminated the sensitivity of pH_i to changes of pH_o (Fig. 2*Bb*).

Dynamic responses of intracellular pH to membrane-permeant weak acids and bases

Superfusion of an individual RBC with NH_4Cl or sodium acetate generated, respectively, a rapid cell alkalinisation and acidification (Fig. 3*A* and *B*). The pH_i then recovered back towards control levels. Similarly, the subsequent

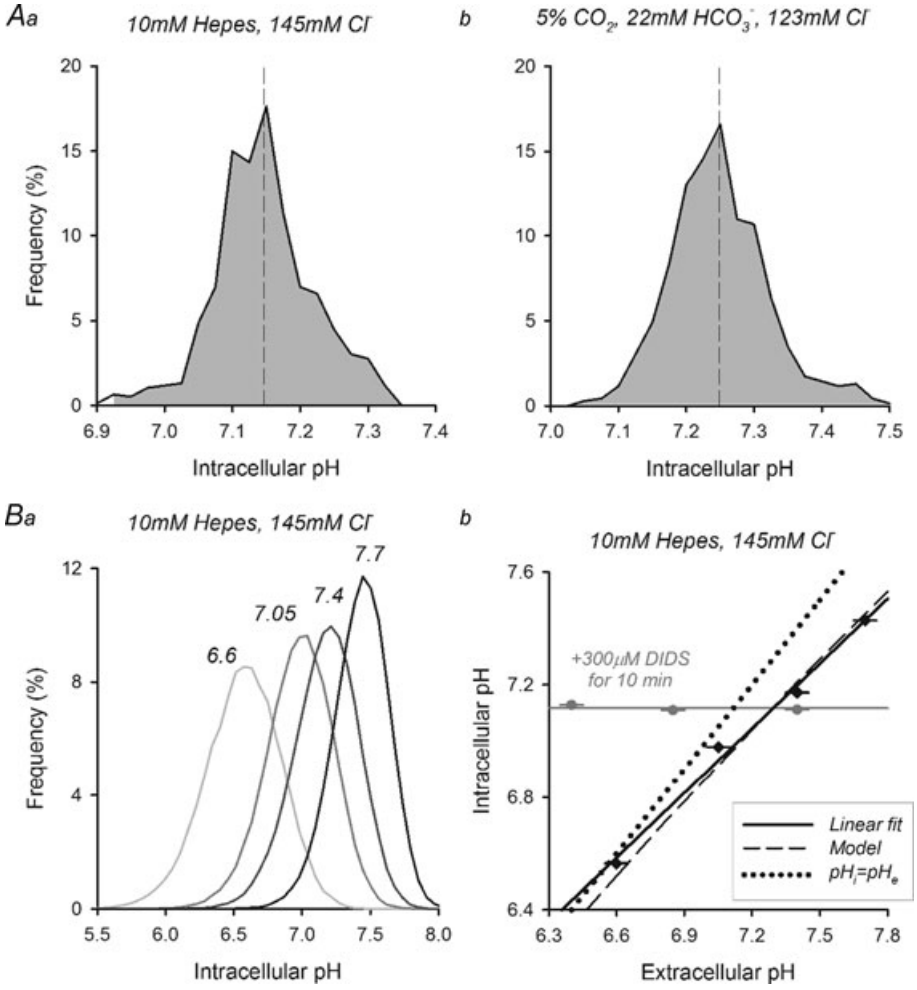

Figure 2. Resting intracellular pH
A, resting pH_i was measured in >700 red cells imaged individually under superfusion with solutions at 37°C, buffered with (*a*) 10 mM Hepes ($[Cl^-]_o = 145$ mM; pH_o 7.4), giving a mean of 7.15 and coefficient of variation (C.V.) 1.02%, or (*b*) 5% CO_2/22 mM HCO_3^- ($[Cl^-]_o = 123$ mM; pH_o 7.4), giving a mean of 7.25 and C.V. of 0.99%. *Bb*, red cells analysed by flow cytometry at 25°C, each data point representing the average of $>10^5$ cells, measured individually. Cells were equilibrated with Hepes-buffered solutions at 25°C of pH at 6.6, 7.05, 7.4 and 7.7. *b*, resting pH_i was linearly dependent on extracellular pH, with a slope of 0.77. The model fit is based on predictions from Lew & Bookchin (1986). Incubation with 300 μM DIDS for 10 min before the change in pH_o produced no effect on pH_i of changing pH_o, indicating that AE1 mediates the response of pH_i to changes in pH_o.

removal of these salts from the superfusate induced, respectively, an intracellular acid load and base load, again followed by a secondary pH_i recovery. The pH_i transients were qualitatively similar when recorded under Hepes- or CO_2/HCO_3^--buffered conditions (Fig. 3*Ab*), although pH_i recovery from acidosis was notably faster with the latter buffer.

The secondary pH_i recovery from the alkalosis induced by ammonium addition (Fig. 3*Aa*), or by acetate removal (Fig. 3*Cb*), was largely abolished when the anion exchange inhibitor DIDS (300 μM) was added to the superfusate. This result indicates a major role for Cl^-/HCO_3^- exchange in restoring pH_i from acute base loading, as similarly reported in many types of eukaryotic cell (Vaughan-Jones, 1982; Aickin, 1994; Sun *et al.* 1996). The absence of a secondary acidification during exposure to ammonium-containing solution in the presence of DIDS also suggests that NH_4^+ entry into cells is minimal. The pH_i recovery from acetate-induced intracellular acidosis (Fig. 3*B*), or from acidosis induced by ammonium-removal (Fig. 3*Ca*), was also blocked by DIDS, implying that AE1 is capable of restoring pH_i from both an acid and an alkaline load. In contrast, pH_i recovery from an acute acid or base load was unaffected by the Na^+/H^+ exchange (NHE) inhibitor dimethyl amiloride (DMA; Fig. 3*Ca* and *b*), suggesting no significant role for this H^+ transporter in RBC pH_i regulation. When combined with previous findings that AE1 is the only known HCO_3^- transporter expressed in RBCs, the present results suggest that pH_i is tightly and symmetrically regulated by the anion exchanger.

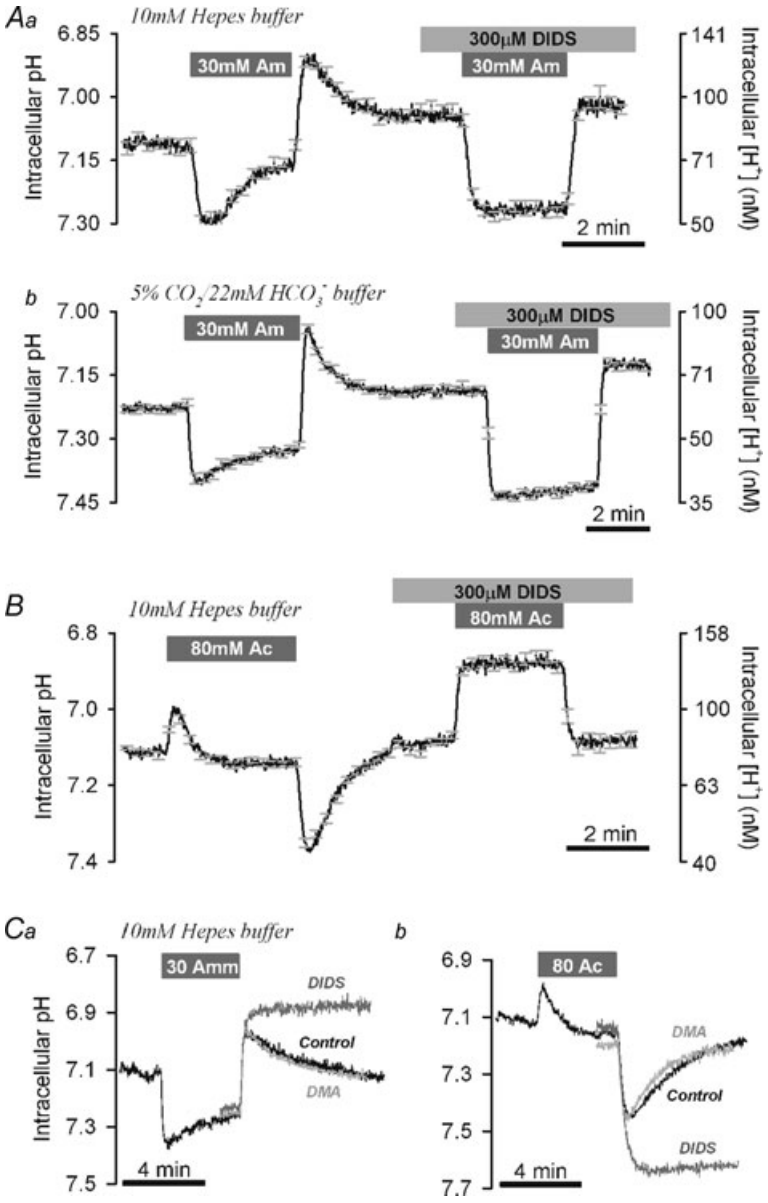

Figure 3. Hydrogen ion dynamics during exposure to salts of weak acid or base
SNARF-1 loaded RBCs were imaged confocally and superfused at 37°C with solutions at pH 7.4. Time courses shown are averages of 5 cells. *A*, transient exposure of cells to solution containing 30 mM ammonium chloride (Am) under (*a*) 10 mM Hepes-buffered or (*b*) 5% CO_2/22 mM HCO_3^--buffered conditions. Ammonium produced an immediate cell-alkalinisation followed by pH_i recovery. On removal of ammonium, the cell acidified and then recovered towards resting pH_i. *B*, transient exposure of cells to solution containing 80 mM sodium acetate (Ac) under 10 mM Hepes-buffered conditions. Acetate produced an immediate cell-acidification followed by pH_i recovery. On removal of acetate, the cell alkalinised and then recovered towards resting levels. Slow pH_i recovery during acetate or ammonium exposure was blocked by the AE1 inhibitor DIDS (300 μM). *C*, recovery of pH_i following (*a*) a 30 mM ammonium prepulse or (*b*) an 80 mM acetate prepulse was not slowed by the Na^+/H^+ inhibitor dimethylamiloride (DMA; 30 μM), but blocked by the AE inhibitor DIDS (300 μM). Drugs were added after ammonium or acetate removal in order to produce adequate acid or base loads for analyses. Averages of 20 cells; error bars omitted for clarity (S.E.M. values < 0.075 pH_i units).

Intrinsic and CO_2/HCO_3^--dependent intracellular buffering capacity

Intracellular H^+-buffering capacity (β) was estimated *in situ* by titrating the cytoplasmic compartment with acid. This was achieved by a stepwise reduction in the concentration of ammonium ions in the superfusate. Figure 4*A* shows that this induced a stepwise fall of pH_i, as intracellular $[NH_4^+]$ was successively depleted via NH_3 efflux, thus depositing intracellular H^+ ions (Boyarsky *et al.* 1988). DIDS was included in all superfusates to block pH_i recovery through AE1. The pH_i steps were used to estimate β (see Methods). Figure 4*B* shows binned data for β ($= -\Delta C_H/\Delta pH_i = \Delta[NH_4^+]_i/\Delta pH_i$), determined from experiments performed in the presence or absence of CO_2/HCO_3^- buffer. In nominally CO_2/HCO_3^--free, Hepes-buffered medium, there was a shallow decline of intrinsic β values over the pH_i range 7.0–7.35, from 100 to 75 mmol (l cell)$^{-1}$ (pH unit)$^{-1}$ (equivalent to 130–100 mmol (l cell water)$^{-1}$ (pH unit)$^{-1}$; assuming water occupies 75% of cell volume; Salenius, 1957; Salminen & Manninen, 1966). Under these conditions, the major intrinsic RBC buffer is haemoglobin, which is rich in H^+-binding histidine residues, with pK values within the physiological pH range.

Intracellular β estimated in the presence of CO_2/HCO_3^- was higher than in Hepes buffered medium (Fig. 4*B*), and was essentially independent of pH_i. The increase in β is due to additional (extrinsic) buffering from intracellular CO_2/HCO_3^-, and was numerically in agreement with that predicted from $[HCO_3^-]_i$, assuming CO_2 instantly equilibrates across the RBC membrane (Roos & Boron, 1981; Leem *et al.* 1999) ($\beta = 2.303 \times [HCO_3^-]_i = 2.303 \times [HCO_3^-]_o \times 10^{7.4\text{-}pHi}$).

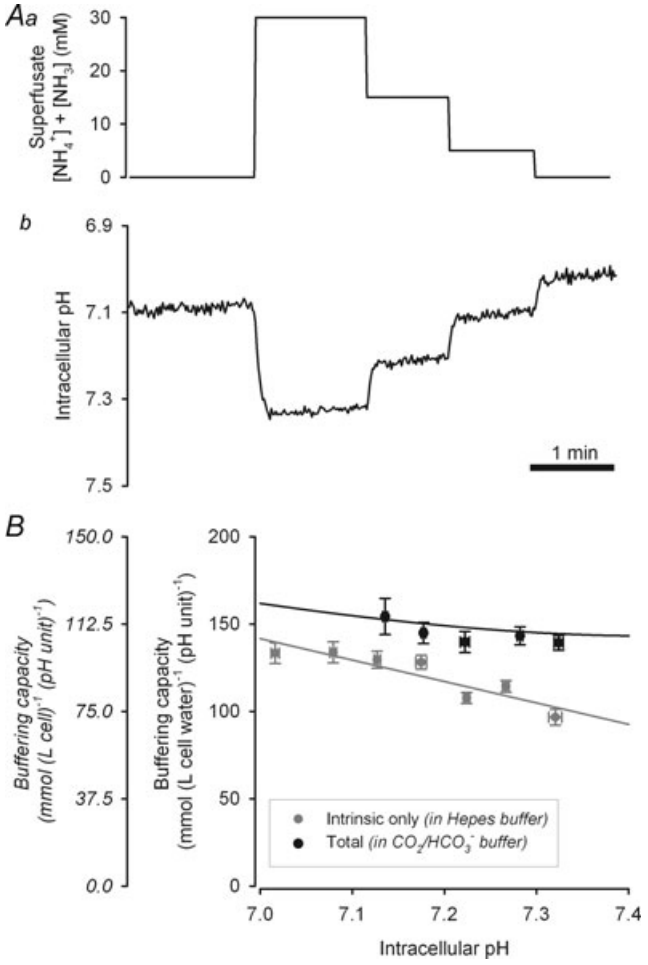

Figure 4. Intracellular pH buffering capacity
A, buffering capacity (β) was measured (at 37°C) using a step-wise ammonium removal protocol (*a*) which produces step-wise changes in pH_i (*b*) (average of 5 cells under Hepes-buffered conditions). *B*, β is plotted under Hepes- and 5% CO_2/22 mM HCO_3^--buffered conditions, which measure intrinsic and total buffering capacity, respectively. The buffering capacity data are presented in units of mmol/(l cell water × pH) (inner axis) or mmol/(l cell × pH) (outer axis in italics), assuming that haemoglobin occupies 25% of cell volume. Each data-point represents the average of >20 cells. The difference in the two data sets is equal to the contribution from CO_2/HCO_3^- buffering ($= 2.303 \times [HCO_3^-]_i$ [mmol/(l cell water × pH)]). Intrinsic β (measured in Hepes buffer) is accounted for by haemoglobin. Best linear fit to intrinsic β is $1000 - 122.64 \times pH_i$ [mmol/(l cell water × pH)].

H^+-equivalent flux through anion exchange and its dependence on intracellular pH

Using estimates of buffering capacity (Fig. 4) and the time courses of pH_i recovery from acid or base loads (Fig. 3*C*), it was possible to characterise the H^+-equivalent flux (J_H) produced by AE1 in the presence or absence of CO_2/HCO_3^- buffer,

$$J_H = -\frac{dpH}{dt} \times \beta$$

Measurements of dpH/dt were made 1 min after the removal of weak acid (acetate) or base (ammonium) to ensure that all intracellular ammonium/acetate has been vented out of cells. Figure 5 shows binned data for J_H, plotted as a function of pH_i (Fig. 5*A*) or intracellular $[H^+]$ (Fig. 5*B*). Flux data obtained in 5% CO_2/22 mM HCO_3^- or Hepes-buffered superfusates are plotted separately. Note that flux is boosted considerably (over fivefold) in the presence of CO_2/HCO_3^- buffer. The dependence of J_H on $[H^+]_i$ is roughly linear, with flux reversal occurring in the region of resting pH_i (72 nM $[H^+]$ in Hepes buffer, and approaching a reversal value of 65 nM $[H^+]$ in CO_2/HCO_3^- buffer). For data gathered in Hepes buffer, the exponent (n) for the best-fit by the function $J_H = a + b \times [H^+]_i^n$ was 0.73, which is close to an exponent of 1.0 (a and b are constants). The near-linearity of the H^+ dependence of flux indicates that the AE1 transporter is not regulated co-operatively by intracellular H^+

ions. The data thus argue for a lack of allosteric control of the transporter by pH_i.

Given that AE1 does not transport H^+ ions directly, the J_H–pH_i relationship shown in Fig. 5*A* most likely describes the substrate dependence of transmembrane H^+-equivalent flux. The H^+-equivalent substrate transported on AE1 is HCO_3^-, probably with no simultaneous transport of OH^- ions (Knauf *et al.* 2002). $[HCO_3^-]_i$ is a function of pH_i and $[CO_2]$. Since $[CO_2]$ was maintained constant during experiments, at either the atmospheric level of 0.04% (with Hepes-buffered superfusates), or at 5% (with CO_2/HCO_3^--buffered superfusates), J_H data were re-plotted and re-binned (Fig. 5*C*) as a function of $[HCO_3^-]$, normalised to $[CO_2]$:

$$\frac{[HCO_3^-]}{[CO_2]} = \frac{K}{[H^+]}$$

where K is $10^{-6.15}$ M. This transformation allows the Hepes and CO_2/HCO_3^- data-sets to be plotted over a comparable x-axis range. The equilibrium condition ($CO_2 + H_2O \rightleftharpoons HCO_3^- + H^+$) that is necessary for this conversion is satisfied by the high intracellular CA activity and by cell superfusion with solutions pre-equilibrated with CO_2/HCO_3^-. The linearity between J_H and the intracellular $[HCO_3^-]/[CO_2]$ ratio confirms that, under conditions where $[Cl^-]_o$ and $[HCO_3^-]_o$ are constant, flux through AE is most likely instructed by $[HCO_3^-]_i$. Although not tested experimentally, deviations from linearity would be expected at high $[HCO_3^-]_i$ due to saturation of binding to the transport site, and possibly at extremes of pH_i, due to changes in $[Cl^-]_i$ that arise from constraints set by the osmotic and electric stability of RBCs.

The time courses of pH_i recovery following an ammonium (Fig. 3*Ca* and 3 *Ab*) or acetate (Fig. 3*Cb*) prepulse, in the absence of DIDS or DMA, are replotted in Fig. 5*D*. These are superimposed with the predicted pH_i time courses derived from the empirical J_H–pH_i relationship (Fig. 5*A*). The good agreement between simulation and experimental data is again consistent with a lack of H_i^+ cooperativity and the ability of AE1 to produce acid or base extrusion depending on the prevailing transmembrane gradients for HCO_3^- and Cl^-.

Response of intracellular pH to changes in extracellular Cl^-

The above results establish that pH_i is efficiently regulated by AE1 (Fig. 3) and can be reset by changing pH_o

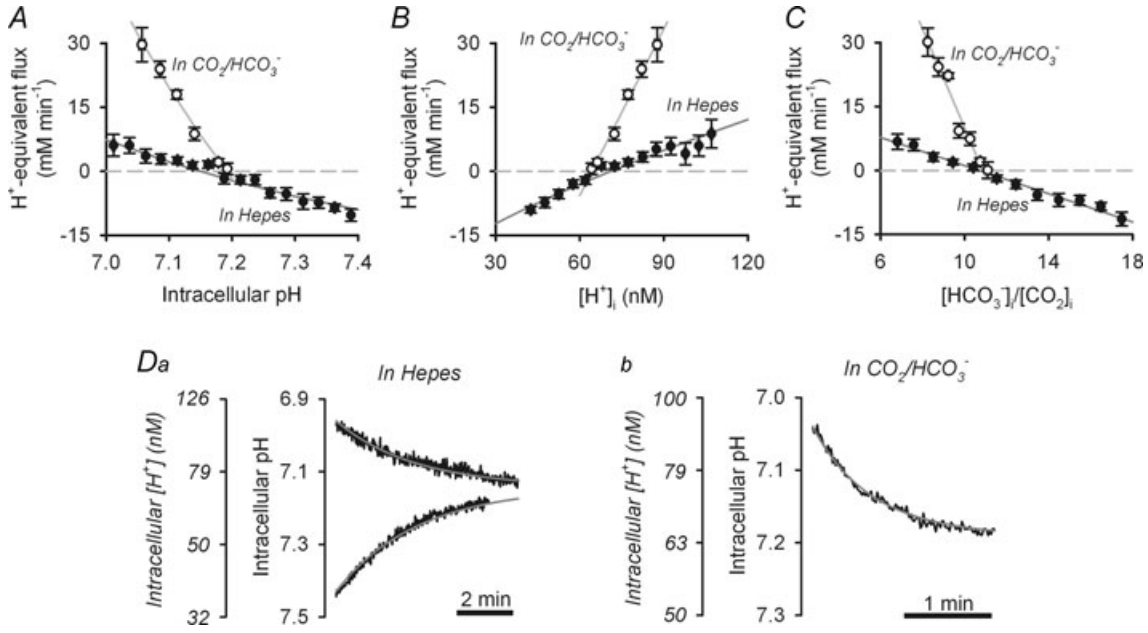

Figure 5. Kinetic characterisation of anion exchange
The pH_i recovery time courses (at 37°C) following ammonium or acetate removal in the absence of DIDS (from Fig. 3) were analysed in terms of H^+-equivalent flux (J_H = slope of pH change × buffering capacity). *A*, J_H plotted as a function of pH_i. The best-fit to a power function ($J_H = a + b \times [H^+]_i^n$) yields an exponent ($n$) of 0.73, suggesting a lack of H_i^+ cooperativity. *B*, J_H plotted against $[H^+]_i$, with the best-fit replotted from *A*. *C*, J_H plotted against the ratio of $[HCO_3^-]/[CO_2]$, which is inversely proportional to $[H^+]$. Since $[CO_2]$ was held constant through each experiment, this x-axis variable is solely dependent on $[HCO_3^-]_i$. The best-fit straight line confirms the linear dependence between substrate concentration and its flux. *D*, the H^+ dependence of J_H and buffering capacity measurements (Fig. 4) were used to reconstruct the pH_i recovery time courses generated by weak acid/base prepulses in the absence (*a*) or presence (*b*) of CO_2/HCO_3^- buffer (data from Fig. 3).

(Fig. 2*B*). Resting pH_i was also sensitive to changes of extracellular $[Cl^-]$. In the experiment shown in Fig. 6*A*, SNARF-1 loaded cells were superfused with an iso-osmotic low-Cl^-, Hepes-buffered solution (100 mM Cl^- replaced by membrane-impermeant gluconate). This manoeuvre generated a reversible intracellular alkalosis that was fully inhibited by DIDS, indicating Cl^- efflux in exchange for HCO_3^- influx through AE1. The initial H^+-equivalent efflux into low Cl_o^- was 15.5 ± 1.0 mM min^{-1}, while initial H^+-equivalent influx on restoration of Cl_o^- was 24 ± 1.2 mM min^{-1}. This asymmetry of flux magnitude, which is consistent with the asymmetry of intracellular *versus* extracellular Cl^- concentration ($[Cl^-]_i > [Cl^-]_o$), agrees well with the predictions (Fig. 6*B*) of a model featuring AE activity that tends to restore equilibrium ($[Cl^-]_o/[Cl^-]_i = [H^+]_i/[H^+]_o$), without allosteric restrictions imposed by H^+ ions. An alkaline-shift in the frequency distribution of resting pH_i upon Cl_o^- reduction, was also measured by flow cytometry after 10 min of gluconate exposure (at 25°C), as shown in the inset.

Extracellular Cl^- reduction was repeated in the presence of CO_2/HCO_3^- buffer (Fig. 6*C*). The reversible alkalinisation was now much faster (probably rate-limited by the data acquisition rate), as expected from the higher concentration of AE1-substrate, HCO_3^- (at pH_o 7.4), and was not blocked completely by DIDS. During the rapid acid efflux associated with Cl^-_o removal, pH_i imaged confocally within individual RBCs remained spatially uniform to within 0.05 pH units (data not shown). This result suggests that cytoplasmic H^+ diffusion is sufficiently fast to maintain spatial pH_i uniformity, even during the

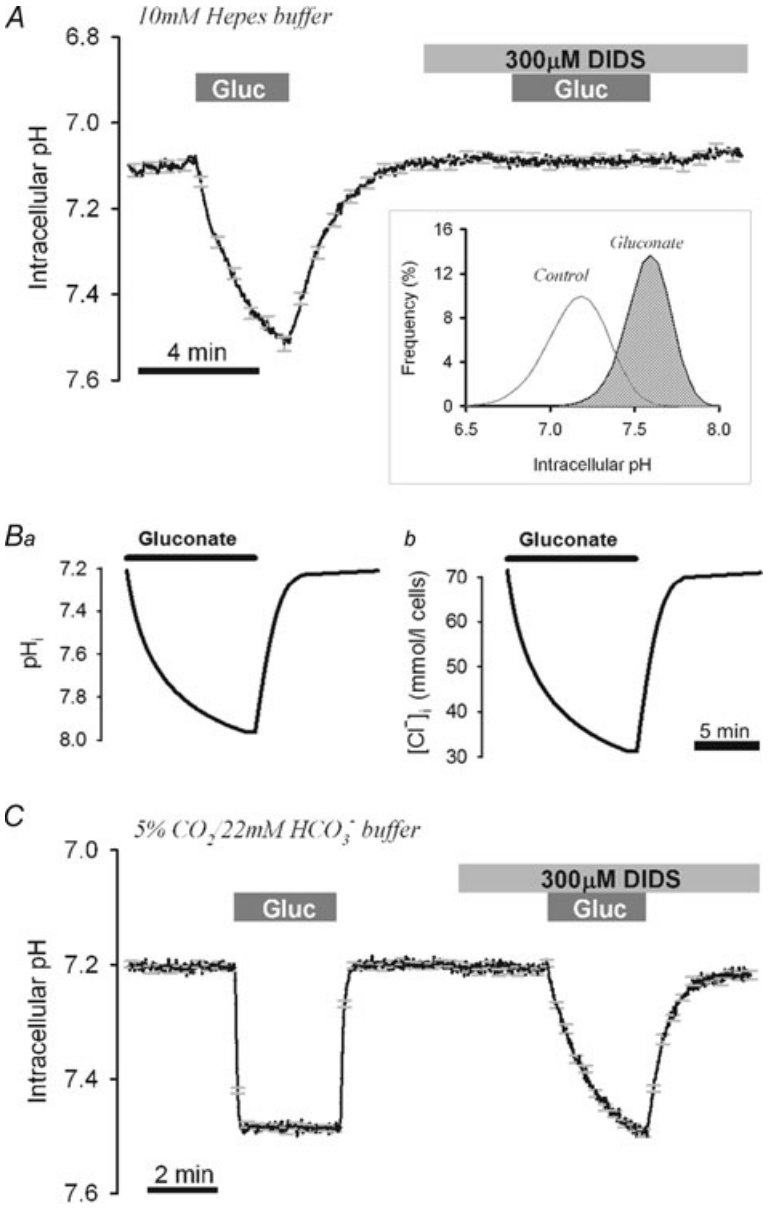

Figure 6. Cell-alkalinisation in response to removal of extracellular chloride
A, RBCs, superfused with Hepes-buffered solutions at 37°C (pH_o 7.4), were exposed to solution in which 100 mM Cl^- was replaced with 100 mM gluconate (Gluc). Rapid reduction in the $[Cl^-]_o/[Cl^-]_i$ ratio towards zero produces a parallel reduction in the $[H^+]_i/[H^+]_o$ ratio (hence cell-alkalinisation) via AE activity. This was abolished by DIDS (300 μM). Inset shows the frequency distribution of pH_i, measured by flow cytometry (Hepes-buffered medium, 25°C, pH_o 7.4), under resting conditions and after 10 minutes following gluconate exposure. *B*, the Lew–Bookchin mathematical model for RBC ionic homeostasis was run to simulate the pH_i response to replacing extracellular Cl^- with gluconate (*a*) and the predicted time course of intracellular $[Cl^-]$ (*b*). *C*, superfusion experiments were repeated with 5% CO_2/22 mM HCO_3^--buffered solutions at 37°C (pH_o 7.4). Cell alkalinisation was considerably faster than in the absence of HCO_3^-, and was slowed, but not blocked completely, by 300 μM DIDS.

large H^+-equivalent transmembrane fluxes recorded in CO_2/HCO_3^- buffer.

Coupling of RBC volume and pH

Possible functional links between the control of RBC pH_i and volume were investigated. To do this, two manoeuvres that influence RBC volume were tested for effects on pH_i: a change of pH_o and an increase in membrane K^+ conductance.

As shown in Fig. 7*Aa*, steady-state RBC volume, measured at pH_o 7.40 by flow cytometry, was normally distributed with a mean value of 89.8 fl and a C.V. of ∼14%. This mean value decreased to 87.0 fl when pH_o was raised to 7.7, and increased to 91.4 fl at pH_o 7.05, and 93.8 fl at pH_o 6.6. The final mean volumes (also normally distributed) are in agreement with previous measurements (Lew *et al.* 1995). A modest decrease of RBC volume thus results from a rise of pH_o over the physiological range. For convenience, the inset reproduces the rise of pH_i that accompanies a rise of pH_o, as also shown in Fig. 2. It is notable that the changes of volume and pH_i were both inhibited by 300 μM DIDS (Fig. 7*Ab*), confirming that modulation of pH_i by pH_o, which is mediated via H^+-equivalent flux through the AE1 transporter, was driving the volume changes. Figure 7*B* combines data from Fig. 7*Ab* and the inset into a single plot, emphasising that cell volume declines by 9% per unit rise of pH_i.

KCl efflux, when activated, also changed volume and pH_i. When fully activated, the Ca^{2+}-sensitive K^+ (Gardos) channel (KCNN4, otherwise known as KCa3.1) of human RBCs can mediate net K^+ efflux that is two orders

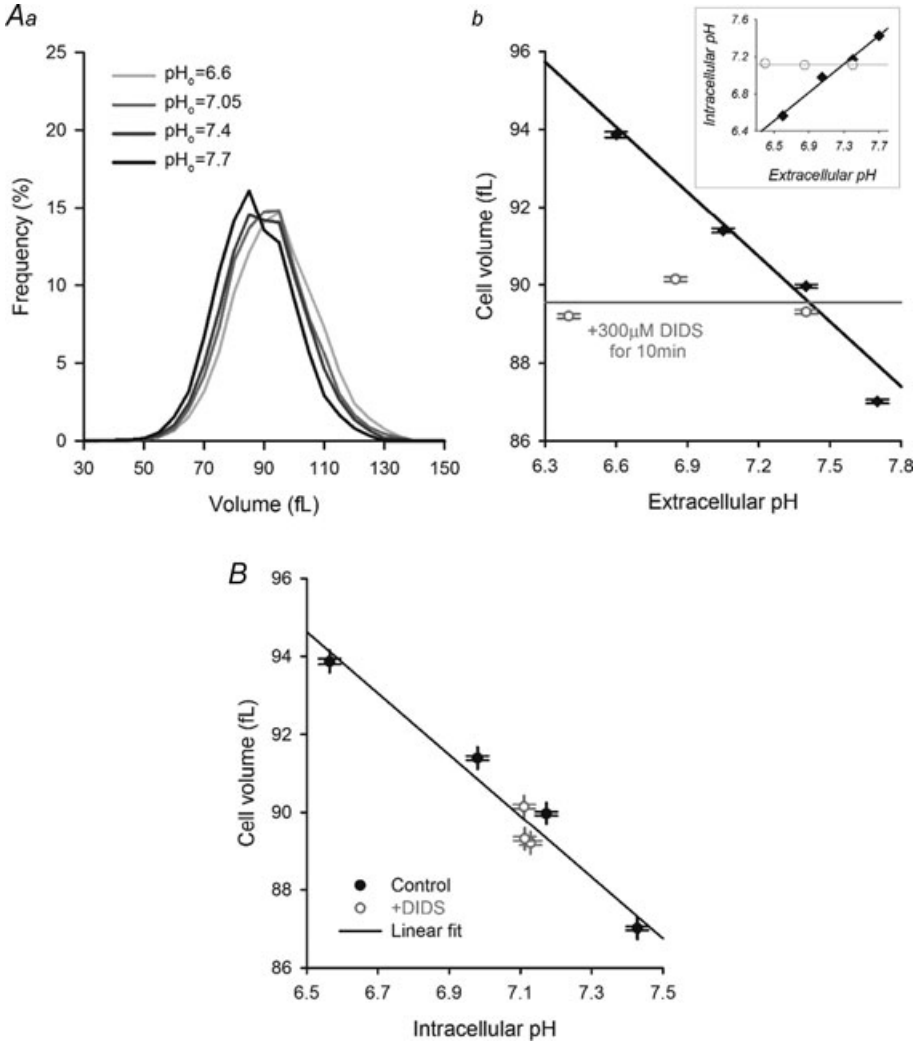

Figure 7. Cell volume is linked with pH_i
Aa, cell volume and pH_i were measured in RBCs bathed in iso-osmotic solutions at different pH_o by flow cytometry at 25°C. *b*, cell volume increased in response to a fall in pH_o. This effect was blocked by 300 μM DIDS, implying a role for AE in the pH_o–volume link. DIDS also collapsed the pH_i–pH_o link (inset). *B*, inverse relationship between pH_i and cell volume, with a slope of −7.9 fl/pH_i.

of magnitude higher than the normal resting K^+ leak (Lew & Ferreira, 1978), and exceeds the restorative capacity of the Na^+/K^+-pump. AE1, operating in ion slippage or tunnelling mode, mediates an electrogenic Cl^- conductance that allows Cl^- efflux to follow the K^+ current. Evidence for electro-diffusional Cl^- flux via AE1 has been derived from the similarity in the sensitivity of electrogenic Cl^- flux and Cl^-/HCO_3^- exchange to stilbene drugs (Kaplan *et al.* 1983; Knauf *et al.* 1983), and the reduced DIDS-sensitive Cl^- conductance in AE knock-out murine RBCs (Alper *et al.* 2008). The loss of water in response to KCl loss leads to RBC dehydration (see Supplemental Fig. S4 for a detailed schematic representation of the underlying flux). The decrease of $[Cl^-]_i$ is then predicted to lower pH_i via AE1-mediated HCO_3^- efflux in exchange for Cl^- influx (Lew & Bookchin, 1986).

To test for a coupling between volume and pH_i during K^+ channel opening, RBCs were superfused with solution B containing 250 μM Ca^{2+} and then exposed to either 1.5 μM ionomycin (a Ca^{2+} ionophore; Fig. 8*Aa*) or 10 μM NS309 (a Gardos channel activator; Fig. 8*Ab*). Intracellular pH and cell volume were recorded confocally from the SNARF-1 fluorescence signals. The pH_i was measured in the usual way, from the SNARF-1 ratio. The fluorescence signal was also used to visualise the outline of an RBC, permitting measurement of its mean diameter in the *xy* plane. Cell dehydration was assessed from the absolute increase in fluorescence intensity, interpolated to the dye's isosbestic wavelength (620 nm). Fluorescence intensity and cell-diameter are only approximate indices of cell volume and therefore their temporal correlation with pH_i must be interpreted with caution. Figure 8*A* illustrates an experiment where the addition of Ca^{2+} ionophore triggered a prompt and progressive intracellular acidification of about 0.14 unit, together with a reduction in cell diameter and a delayed increase in SNARF-1 fluorescence intensity, both indicative of progressive cell dehydration. K^+ channel opening thus decreased cell volume and pH_i. The cause of the small initial fall in overall fluorescence intensity upon K^+ channel opening, which preceded the fluorescence increase (Fig. 8*Aa*, lower panel), is not known. It may be due to a decrease in overall fluorescence yield during acidification. The apparently delayed response of cell diameter, relative to acidification, may reflect a change in volume along the *z*-axis that is not reflected in the *xy* plane. The sustained change in cell diameter and fluorescence intensity after pH_i had stabilised at a new acidic level may reflect changes in cell shape at constant volume (Cueff *et al.* 2010). Nevertheless, the combined measurement of cell diameter and intracellular fluorescence intensity provides a good, albeit semi-quantitative indication of cell dehydration.

NS309 is a well characterized positive modulator of Gardos channels (Strobaek *et al.* 2004; Baunbaek & Bennekou, 2008). It acts by increasing the Ca^{2+} sensitivity of the channels, such that they become capable of dehydrating RBCs at physiological or even sub-physiological $[Ca^{2+}]_i$ (<50 nM) (Baunbaek & Bennekou, 2008). The effect of NS309 on RBC volume and pH is shown in Fig. 8*Ab*. Again, cell dehydration, monitored confocally, was associated with an intracellular acidification of ~0.1 units. The pH_i and volume responses to ionomycin and NS309 were both abolished by blocking AE1 with DIDS (Fig. 8*Ba* and *b*), implying a role for AE1 in the volume–pH_i coupling.

Further experiments were performed with flow cytometry to obtain the steady-state relationship between pH_i and cell volume during K^+ channel activation. Figure 8*C* plots population-averaged data, under control conditions and in the presence of NS309 or ionomycin, after allowing 15–30 min for the drugs to exert their effects. During K^+ channel activation, a 0.1 unit fall of pH_i from its resting level (7.17) was associated with a 20% decline in cell volume. To augment the effect of NS309, one set of experiments was performed in the presence of the Ca^{2+} pump inhibitor, 1 mM vanadate, to raise intracellular $[Ca^{2+}]$. Vanadate potentiated the effect of NS309, producing a more dehydrated and more acidic population of RBCs (Fig. 8*C*). This finding also suggests that, under control conditions, the Ca^{2+} pump remains functional in the presence of intracellular SNARF-1, as suggested earlier (see also Supplemental Fig. S1).

In summary, direct measurements of RBC pH_i indicate that it changes significantly during manoeuvres that influence cell volume. The direction of pH_i change, however, depends on the underlying cause of the volume change. RBC shrinkage induced by extracellular alkalinisation is associated with a rise of pH_i, whereas shrinkage induced by K^+ channel activation reduces pH_i. In both cases, AE1 transport activity drives the pH_i change.

Discussion

The present work reports the first direct recordings of pH_i in individual RBCs. The measurements have permitted a characterisation of pH_i regulation in these cells, and its functional coupling to mechanisms that regulate cell volume. The results highlight the RBC's exceptionally high intracellular buffering capacity, the unusual role of the AE1 gene product as both an acid and a base extruder following cytoplasmic acidosis or alkalosis, and the occurrence of AE1-driven pH_i signals during cell shrinkage or swelling. Intracellular pH is thus tightly regulated in the RBC, but modulated by the cell's volume.

Resting pH_i in the human RBC

The mean resting pH_i of 7.25 (i.e. less than pH_o 7.4) is consistent with previous indirect estimates (Jacobs & Stewart, 1947; Salenius, 1957; Salminen & Manninen, 1966; Dalmark, 1975), the value becoming somewhat more acidic (7.15) in the nominal absence of physiological CO_2/HCO_3^- buffer. The more alkaline pH_i in the presence of CO_2/HCO_3^- buffer cannot be explained by differences

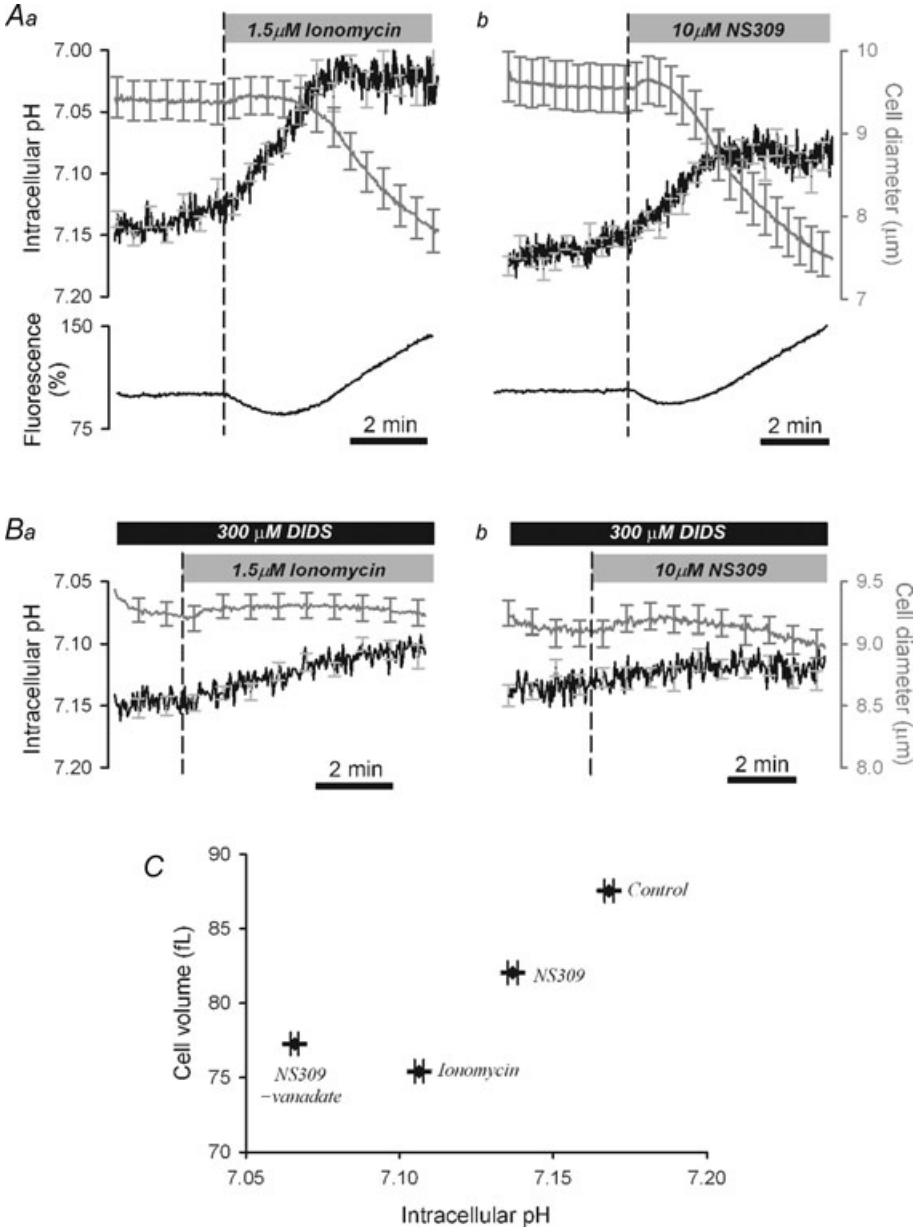

Figure 8. Cell dehydration is linked to cell acidification during activation of K^+ conductance
Cells were superfused in Hepes-buffered solution containing 10 mM NaSCN (to accelerate AE turnover) and 250 μM $CaCl_2$. *A*, confocal imaging under superfusion (at 37°C). (*a*), addition of 1.5 μM ionomycin activated Ca^{2+}-sensitive K^+ channels, which triggered cell dehydration (due to KCl and water loss), as measured from the SNARF-fluorescence density (interpolated to the isosbestic wavelength of 620 nm; lower panel) and mean cell diameter (grey trace, upper panel). This was accompanied by cell acidification, as measured from the calibrated SNARF-1 ratio (black trace, upper panel). (*b*), a similar observation was made using 10 μM NS309, a drug that sensitises Ca^{2+}-sensitive K^+ channels to open at resting $[Ca^{2+}]_i$. *B*, the response to ionomycin or NS309 was blocked by 300 μM DIDS, the AE inhibitor, implying a central role of AE in mediating the dehydration/acidification response. Each time course is the average of >20 cells. *C*, flow cytometry analysis of cell volume and pH_i (at 25°C) in cells equilibrated in control medium (with SCN^- and Ca^{2+}) or treated with ionomycin (1.5 μM), NS309 (10 μM) or NS309 with vanadate (1 mM; to raise $[Ca^{2+}]_i$). Flow cytometry confirms the link between pH_i and volume.

in Hb oxygenation as all media were in equilibrium with atmospheric air. The reason for the lower pH_i in Hepes buffer was not investigated further, but may be related to the presence of membrane-impermeant, anionic Hepes or a greater degree of haemoglobin ionisation in the absence of intracellular HCO_3^- and/or CO_2. The low C.V. for the resting pH_i frequency distribution (1%; see Fig. 2) indicates a high degree of pH_i homogeneity among cells (measured with confocal imaging at 37°C and flow cytometry at 25°C). This homogeneity persists when pH_o is displaced from its normal value of 7.4, causing pH_i to settle at a new level, but still with a low C.V. Measurements of average pH_i within a suspended population of RBCs have been reported previously (mean pH_i ~7.10 at pH_o 7.4), using intracellular BCECF fluorescence in nominally CO_2/HCO_3^--free conditions (Kummerow *et al.* 2000). In that work, however, pH_i estimates were not based on individual RBC measurements, and the *in situ* nigericin calibration was not validated against an independent (null-point) method so that, as emphasised below, possible measurement errors cannot be excluded.

SNARF-1: suitable for pH measurement in RBCs, but only with null-point calibration

The high quantum yield of AM-loaded SNARF-1 in the RBC appears to overcome the quenching power of intracellular haemoglobin, which has been shown to attenuate the fluorescence signal from other ion-sensitive fluorophores, such as the Ca^{2+} indicators Fura-2 and Indo-1 (Lew *et al.* 1993; Kaestner *et al.* 2006). Intracellular loading of SNARF-1 also has no effect on resting RBC volume (Supplemental Fig. S1), suggesting that the dye does not disrupt Ca_i^{2+} and cell volume homeostasis. SNARF-1 may thus be preferable to BCECF for pH_i measurement, as the latter fluorophore is believed to inhibit the plasma membrane Ca^{2+} pump (Gatto & Milanick, 1993).

The SNARF-1 ratio in RBCs was calibrated using two independent approaches (Fig. 1). The null-point approach produced a pH_i calibration curve that was acid-shifted relative to the more commonly used nigericin method (Fig. 1*C*). Due to the presence of intracellular haemoglobin, $[Cl^-]_i < [Cl^-]_o$ and therefore pH_i is expected to be more acidic than pH_o when AE1 is at equilibrium. The null-point calibration produced an estimate of RBC resting pH_i (7.15–7.25) that was in agreement with this equilibrium condition, whereas the nigericin method erroneously suggested parity between resting pH_i and pH_o. A similar discrepancy between nigericin and null-point calibrations has been reported previously for renal mesangial cells (Boyarsky *et al.* 1996), but not for other cell types, such as carotid body glomus cells and cardiac myocytes (Buckler & Vaughan-Jones, 1990; Leem *et al.* 1999), or in the three epithelial cell-lines tested in the present work (Supplemental Fig. S3).

The reason for the calibration discrepancy in RBCs is not clear and requires further investigation. However, it is noteworthy that a significant fraction of RBCs was observed to haemolyse spontaneously in the presence of nigericin. Cells that remain intact under these conditions and provided data for the nigericin calibration curve may therefore represent a subset of cells that is not representative of the whole population. Another possibility is that, when exposed to nigericin, these RBCs do not reach a true steady-state in terms of cell volume and ionic composition. In such a quasi-stable state, transmembrane K^+ and H^+ gradients may be unequal, thus biasing the nigericin curve. The similarity between nigericin calibrations of RBC pH_i obtained with 100 mM and 140 mM K^+_o suggests that the error does not simply arise as a result of inappropriate matching of extracellular to intracellular $[K^+]$, but may involve factors that are unique to RBCs, such as direct nigericin effects on membrane stability. Significant haemolysis did not occur in RBCs during null-point calibration, and resting pH_i values so derived appeared to be accurate, given that experimental measurements of intracellular CO_2/HCO_3^--dependent buffering agreed quantitatively with theoretical predictions, a result that would not occur if estimates of pH_i were in error (see also Boyarsky *et al.* 1996 for a discussion of this point). When quantifying pH_i in the RBC, the nigericin technique for *in situ* pH fluorophore calibration should thus be abandoned in favour of the null-point method.

Intracellular H^+-buffering in human RBCs

The ability to record pH_i permitted the application of an extracellular ammonium-withdrawal technique for estimating buffering capacity directly within the RBC, as illustrated in Fig. 4 (Boyarsky *et al.* 1988). The resulting value for intrinsic (non-CO_2/HCO_3^--dependent) buffering capacity (in excess of 100 mmol (l cell water)$^{-1}$ (pH unit)$^{-1}$) is among the highest observed in any cell type. This is consistent with the high concentration of intracellular haemoglobin, a high-capacity pH buffer (the mean Hb concentration of 5.2 mmoles per litre of packed cells, is equivalent to 7.0 mmol (l cell water)$^{-1}$, assuming that 25% of the cell volume is occupied by Hb molecules) (Lew *et al.* 1991). Intracellular Hb buffering capacity has previously been estimated from acid-titration of cell-lysates to be between 53 and 68 mmol (l cell)$^{-1}$ (pH unit)$^{-1}$ (equivalent to 70–91 mmol (l cell water)$^{-1}$ (pH unit)$^{-1}$; (Cass & Dalmark, 1973; Dalmark, 1975). The present *in situ* estimate of intrinsic buffering is thus at least 11% higher than previous indirect estimates, and possibly up to 50% higher, depending on the pH_i at

which β-values are selected (Fig. 4). The discrepancy may indicate the presence of intracellular RBC buffers in addition to haemoglobin, or may point to previous errors in estimates of the proportion of cell volume occupied by water. Alternatively, the assumptions involved in the ammonium-withdrawal method for estimating β may not apply in RBCs.

Measurements of buffering capacity in the presence of physiological CO_2/HCO_3^- buffer reveal an additional component of RBC buffering, derived from intracellular CO_2/HCO_3^- (Fig. 4*B*), which has not previously been quantified. The ability of CO_2/HCO_3^- to buffer pH_i changes is limited by the kinetics of the chemical reaction $CO_2 + H_2O \rightleftharpoons HCO_3^- + H^+$. High intrinsic buffering due to intracellular Hb will tend to slow equilibration of this reaction, and therefore sufficient catalysis by the high levels of intracellular CA is required to enable CO_2/HCO_3^- buffering to operate efficiently (Meldrum & Roughton, 1933; Maren, 1967). The present measurements show that intracellular CO_2/HCO_3^- can contribute up to a third of total buffering power within the RBC over the physiological pH_i range. The close agreement between experimentally derived values for this component of buffering and the theoretical values (predicted to be 2.303 $\times$ $[HCO_3^-]_i$ in an intracellular compartment fully open to extracellular CO_2; see Fig. 4*B* and Roos & Boron, 1981) suggests that the ammonium-withdrawal technique for measuring RBC buffering capacity is accurate.

pH_i regulation in human RBCs

The present work shows that acute displacement of pH_i in the acid or alkaline direction is compensated within a few minutes by acid or base extrusion from the cell. The system superficially resembles that observed in most eukaryotic cells. In the case of the RBC, however, the principal pH_i sensor and transport effectors are subsumed within a single type of membrane protein, the AE1 Cl^-/HCO_3^- exchanger.

In eukaryotic cells, major acid and base effluxes are typically mediated via separate membrane transport proteins, such as Na^+/H^+ exchange (H^+ efflux) and Cl^-/HCO_3^- exchange (H^+-equivalent influx) (Boron, 2004; Vaughan-Jones *et al.* 2009). NHE1 transcripts have been reported in immature RBCs (reticulocytes that comprise ~1% of an RBC population) (Sarangarajan *et al.* 1998), and an amiloride-sensitive $^{22}Na^+$ uptake has been measured in human RBCs (Escobales & Canessa, 1986). In the present work, however, exposure of RBCs to the NHE inhibitor, dimethyl amiloride, had no effect on pH_i recovery from an acid load, while exposure to DIDS, an AE1 inhibitor with no potency against NHE1, blocked acid extrusion completely (Fig. 3*Ca*). While these results do not exclude the appearance of significant NHE1 activity in certain clinical conditions, like hyperaldosteronism (Koren *et al.* 1998), they indicate little or no role for the transporter in the regulation of pH_i in normal mature RBCs. AE1 is a product of the SLC4 gene family of bicarbonate transporters (SLC4A1). A second gene family (SLC26) also codes for anion exchange transport proteins (Sterling & Casey, 2002; Mount & Romero, 2004), but its products have not so far been identified in RBCs, so that AE1 remains the only candidate HCO_3^- transporter. The human mature RBC is thus unusual in that all aspects of transmembrane pH_i regulation seem to be accomplished by AE1. As discussed below, this arrangement works successfully for two reasons: (i) AE1 is at ionic equilibrium at resting pH_i (i.e. $[HCO_3^-]_o/[HCO_3^-]_i = [Cl^-]_o/[Cl^-]_i = [H^+]_i/[H^+]_o$), and (ii) AE1 activity is not allosterically modulated by pH_i.

In other cell types, transporters such as NHE and Cl^-/HCO_3^- exchange are typically far from ionic equilibrium at resting pH_i, and so are constrained thermodynamically to produce only H^+-equivalent efflux or influx in the physiological pH_i range. In contrast, because it is normally at ionic equilibrium, AE1 in the RBC can operate reversibly, producing acid influx or efflux (Fig. 5*A*).

The activity of NHE and Cl^-/HCO_3^- exchangers in non-erythroid cells is typically modulated allosterically by H^+ ions, so that acid/base transport is high only over a narrowly defined range of pH_i, sometimes resulting in a preferred polarity for H^+-equivalent flux across the membrane i.e. flux rectification (Aronson *et al.* 1982; Olsnes *et al.* 1986; Leem *et al.* 1999). In contrast, the present results in the RBC provide no evidence for allosteric pH modulation of AE1, so that significant activity is observed at both acid and alkaline pH_i (Fig. 5*A*). A lack of allosteric restraint also helps to explain the high dependence of steady-state pH_i in the RBC on changes of pH_o, a relationship defined by H^+-equivalent (HCO_3^-) flux through the AE1 transporter (Fig. 2*Bb*). The transfer function ($\Delta pH_i = 0.77 \times \Delta pH_o$) is the steepest measured for any cell type. For example, a typical pH_i/pH_o slope of ~0.4 has been reported in cardiac cells (Ellis & Thomas, 1976; Sun *et al.* 1996) while in *Xenopus* oocytes (Humphreys *et al.* 1994) it is 0.14. The equilibrium value of pH_i will also be responsive to changes in $[Cl^-]_i$ and $[Cl^-]_o$ (Fig. 6). Consequently, any changes to the net ionisation state of haemoglobin, such as those arising from changes in oxygenation status (Tiffert *et al.* 1993), will alter pH_i via changes in $[Cl^-]_i$.

The present work shows that AE1 transport activity in the RBC correlates linearly with $[HCO_3^-]_i$, the concentration of transported substrate (Fig. 5*C*). As a result, the relationship between pH_i and J_H is also approximately linear (Fig. 5*A*). The pH_i sensitivity of AE1 activity is thus likely to be more apparent than

real, reflecting instead a first-order dependence on $[HCO_3^-]_i$. This conclusion is consistent with the broad pH insensitivity of $^{36}Cl^-$ flux previously reported for AE1 in red cell ghosts (Funder & Wieth, 1966), and in heterologous expression systems (Zhang *et al.* 1996). AE1 is likely to regulate RBC pH_i by sensing an associated rise or fall of $[HCO_3^-]_i$ (via its intracellular anion binding site), and adjusting HCO_3^- transport accordingly. These kinetic properties are very different from other anion exchange isoforms of the SLC4 gene family, such as AE2 and AE3, which are allosterically switched down at low pH_i (Lee *et al.* 1991; Stewart *et al.* 2004). The present results therefore suggest that pH_i regulation in the RBC may be the beneficial consequence of a system evolved to regulate $[HCO_3^-]_i$. This is perhaps to be expected as AE1's prime role is to translocate HCO_3^- in either direction across the RBC membrane during the mass transport of CO_2 from respiring tissue to lungs. HCO_3^- flux reversal during this cycle is aided by a transporter close to equilibrium at resting pH_i, and without allosteric restraint. This design, nevertheless, means that RBC pH_i can, when required, be efficiently controlled, as shown in the present work. This is desirable, as the RBC's protein machinery, including its Hb and its glycolytic and CA enzymes are all H^+ sensitive, with a proscribed pH_i range for optimal function.

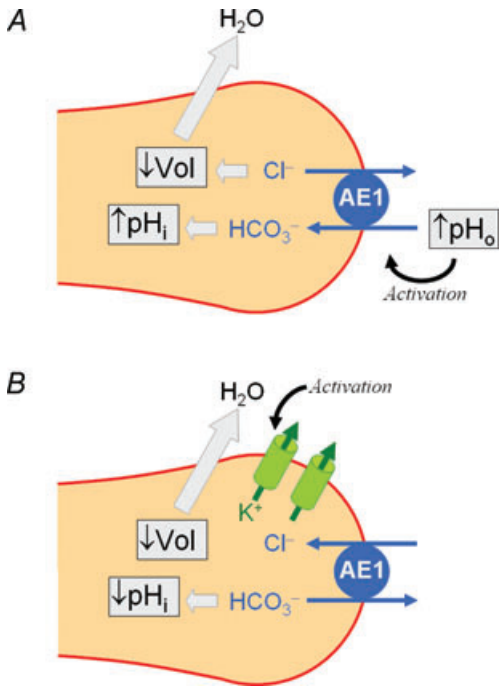

Figure 9. Schematic model of the link between cell volume and pH_i
A, activation of Cl^- efflux/HCO_3^- influx through AE by high pH_o (inward $[HCO_3^-]$ gradient) produces an alkalinisation of the cell and loss of intracellular Cl^-. Cell volume decreases due to water exit, because the fall in $[Cl^-]$ is not osmotically balanced by the rise in $[HCO_3^-]$ (as a result of H^+-buffering). Cl^-/HCO_3^- exchange in parallel with CO_2 permeation is equivalent to H^+–Cl^- co-transport, which is capable of driving osmolyte fluxes. *B*, activation of Ca^{2+}-sensitive K^+ conductance triggers K^+ efflux, followed by Cl^- efflux and water loss. This dehydrates the cell and also reduces the intracellular $[Cl^-]$ concentration (and raises the concentration of haemoglobin, Hb, the principal membrane-impermeant anionic species). The rise in the $[Cl^-]_o/[Cl^-]_i$ ratio produces intracellular acidification by the activity of anion exchange.

DIDS-sensitive pH_i regulation in the RBC is still evident in the nominal absence of CO_2/HCO_3^- (Fig. 3*Aa*, *B* and *C*), albeit at a much slower rate (Fig. 3*Ab*), raising the possibility that OH^- may be transported as well as HCO_3^-, particularly when levels of the latter are low. While this occurs for H^+-equivalent transport on certain SLC26 gene products (Alvarez *et al.* 2004, but see Knauf *et al.* 2001), kinetic analyses have suggested that AE1, an SLC4A1 gene product, does not transport OH^-, but operates instead on residual HCO_3^- levels (Papageorgiou *et al.* 2001; Knauf *et al.* 2002). Because of the presence of atmospheric CO_2, intracellular and extracellular $[HCO_3^-]$ are constitutively in the range 100–350 μM (and will vary with pH), which appears to be sufficient to support a low level of AE1 activity (Knauf *et al.* 2002). Rapid pH_i regulation in the RBC is thus likely to be dependent on the transport of HCO_3^-, and regulated by its ambient concentration.

pH_i–volume coupling in human RBCs

Although pH_i is tightly regulated, it is nevertheless modulated by changes of RBC volume. In some cases the volume change may be driven directly through AE1 activity. For example, raising pH_o (at constant CO_2 partial pressure) induces a modest cell shrinkage by driving H^+ and Cl^- efflux through AE1 (equivalent to Cl^- efflux/HCO_3^- influx), which raises pH_i (Fig. 7). Cell dehydration occurs (Fig. 7) because the ensuing $[Cl^-]_i$ reduction is not balanced by an osmotically equivalent rise of $[HCO_3^-]_i$ (owing to intracellular H^+-buffering). The primary activation of cell dehydration via AE1 is thus linked directly with intracellular alkalosis, as illustrated schematically in Fig. 9*A*. Another example of this type of pH_i–volume coupling would be activating AE1 by reducing $[Cl^-]_o$ at constant extracellular osmolarity (replacing extracellular Cl^- with a membrane-impermeant anion). As shown in Fig. 6, this raises pH_i as Cl^- exits from the RBC in exchange for HCO_3^- via AE1. The reaction between intracellular HCO_3^- and H^+ ions yields CO_2 which exits cells freely. Consequently, Cl^- efflux produces a net loss of osmolyte, which is accompanied by water loss and cell shrinkage (Lew & Bookchin, 1986).

In contrast to the effects of directly activating AE1, induction of KCl efflux through the opening of KCNN4 (KCa3.1) Gardos channels in the surface membrane is a powerful primary stimulus for cell dehydration, directly

inducing an osmotic efflux of water. By reducing $[Cl^-]_i$, the KCl loss disturbs the AE1 transporter's equilibrium state, resulting in a Cl^- influx/HCO_3^- efflux, as predicted by the RBC model (Lew & Bookchin, 1986). The cell thus acidifies, as illustrated in Fig. 9*B* (a more detailed schematic representation of the underlying ionic changes is available in Supplemental Fig. S4). In this case, the primary activation of cell dehydration through KCl efflux then induces a secondary acidosis through AE1. Thus, manoeuvres that alter RBC volume also induce a change of pH_i. But depending on whether Cl^-/HCO_3^- exchange is the primary cause of the volume change (Fig. 9*A*), or is activated secondarily (Fig. 9*B*), the pH_i signals move in opposite directions. Nevertheless, through recruitment of AE1 activity, volume changes in the RBC are inevitably coupled to pH_i changes. In effect, the equilibrium condition for pH_i regulation by AE1 is reset to a new resting pH_i by a volume disturbance.

Under physiological conditions, Ca^{2+}-activated KCNN4 channels are silent, except perhaps in ageing cells with slightly elevated $[Ca^{2+}]_i$ where they may be minimally activated, contributing to the homeostatic changes observed during RBC senescence (Lew *et al.* 2007; Tiffert *et al.* 2007). In certain diseased states, such as sickle-cell anaemia, the channels play a key role in disease pathogenesis, and their activation leads to the formation of a subpopulation of young, hyperdense and irreversibly sickled red cells (Lew & Bookchin, 2005). The combination of cell dehydration and cell acidification was proposed as a critical link in the generation of these hyperdense cells (Lew *et al.* 1991). Measurements of extracellular pH have indirectly supported the existence of this volume–pH_i coupling and an involvement of anion exchange (Freeman *et al.* 1987). Mathematical modelling of RBC ion homeostasis also predicts volume–pH_i coupling. The present work now provides the first direct measurement of the coupling, and confirms the central role of AE1.

Conclusions

Imaging pH_i confocally in individual RBCs, as well as profiling it in large populations using flow cytometry, provides a new tool for exploring hydrogen ion dynamics in erythrocytes, in both health and disease. As with other cells, an efficient control of pH_i in the RBC is necessary for the maintenance of normal activity. Furthermore, the functional coupling between volume and pH_i recorded in the present work need not be exclusive to the erythrocyte. It may be applicable to any cell type that expresses Cl^-/HCO_3^- exchange at the surface membrane (including products of the SLC26 as well as the SLC4 gene families). The amplitude of the volume-associated pH_i signal will depend, in part, on the kinetic properties of the anion exchanger, as well as on the co-expression and functional activity of other plasmalemmal acid/base extruders. In some cells, a functional coupling between anion exchange and Na^+/H^+ exchange results in pH_i-neutral volume regulation (Mason *et al.* 1989). Nevertheless, the principle that the anion exchanger can also couple changes of cell volume to a significant pH_i signal should not be ignored when considering the integrated response of a cell.

Appendix

The null-point method for calibrating pH sensitive dyes has been discussed in detail elsewhere (Eisner *et al.* 1989; Buckler & Vaughan-Jones, 1990). The method assumes that cell entry of the charged form of weak acid/base (acetate Ac^-, ammonium NH_4^+) is negligible over the time period tested. This is supported by pH_i time course data in the presence of DIDS (Fig. 3). Exposure to ammonium-containing solution (Fig. 3*A*) produces an intracellular alkalinisation (NH_3 entry) with no secondary acidification (i.e. no NH_4^+ entry). Similarly, exposure to acetate-containing solution (Fig. 3*B*) produces acidification (acetic acid entry) but no secondary alkalinisation. A certain combination of weak acid (acetate/acetic acid) and weak base (ammonium/ammonia) produces no net change in pH_i at steady-state. At this pH_i, $[NH_4^+]_i = [Ac^-]_i$. Assuming that weak acid/base ionisation constants are the same on either side of the membrane, it is possible to derive a relationship linking pH_o, the concentration of weak acid ($T_A = [Ac^-]_o + [HAc]_o$), weak base ($T_B = [NH_3]_o + [NH_4^+]_o$) and the null point pH_i (pH_{null}):

$$\sqrt{\frac{T_B}{T_A}} = \frac{[H^+]_o}{[H^+]_i} = 10^{pH_{null} - pH_o}$$

When no change in steady-state dye fluorescence is observed in a cell superfused with weak acid and base, in a ratio equal to T_B/T_A, resting pH_i (i.e. pH_{null}) can be derived from the equation above. The null-point calibration time courses produce initial, transient alkaline displacements of pH_i, before attaining a steady-state pH_i, because NH_3 is more membrane permeant than the large HAc molecule. However, the derivation above relates to the steady-state condition, once NH_3 and HAc have attained equal transmembrane distribution.

References

Aickin CC (1994). Regulation of intracellular pH in the smooth muscle of guinea-pig ureter: HCO_3^- dependence. *J Physiol* **479**, 317–329.

Alper SL (1991). The band 3-related anion exchanger (AE) gene family. *Annu Rev Physiol* **53**, 549–564.

Alper SL, Vandorpe DH, Peters LL & Brugnara C (2008). Reduced DIDS-sensitive chloride conductance in Ae1–/– mouse erythrocytes. *Blood Cells Mol Dis* **41**, 22–34.

Alvarez BV, Kieller DM, Quon AL, Markovich D & Casey JR (2004). Slc26a6: a cardiac chloride–hydroxyl exchanger and predominant chloride–bicarbonate exchanger of the mouse heart. *J Physiol* **561**, 721–734.

Aronson PS, Nee J & Suhm MA (1982). Modifier role of internal H^+ in activating the Na^+–H^+ exchanger in renal microvillus membrane vesicles. *Nature* **299**, 161–163.

Baunbaek M & Bennekou P (2008). Evidence for a random entry of Ca^{2+} into human red cells. *Bioelectrochemistry* **73**, 145–150.

Begenisich T, Nakamoto T, Ovitt CE, Nehrke K, Brugnara C, Alper SL & Melvin JE (2004). Physiological roles of the intermediate conductance, Ca^{2+}-activated potassium channel Kcnn4. *J Biol Chem* **279**, 47681–47687.

Bookchin RM, Ortiz OE & Lew VL (1991). Evidence for a direct reticulocyte origin of dense red cells in sickle cell anemia. *J Clin Invest* **87**, 113–124.

Boron WF (2004). Regulation of intracellular pH. *Adv Physiol Educ* **28**, 160–179.

Boyarsky G, Ganz MB, Sterzel RB & Boron WF (1988). pH regulation in single glomerular mesangial cells. I. Acid extrusion in absence and presence of HCO_3^-. *Am J Physiol Cell Physiol* **255**, C844–856.

Boyarsky G, Hanssen C & Clyne LA (1996). Inadequacy of high K^+/nigericin for calibrating BCECF. I. Estimating steady-state intracellular pH. *Am J Physiol Cell Physiol* **271**, C1131–1145.

Buckler KJ & Vaughan-Jones RD (1990). Application of a new pH-sensitive fluoroprobe (carboxy-SNARF-1) for intracellular pH measurement in small, isolated cells. *Pflugers Arch* **417**, 234–239.

Cabantchik ZI & Rothstein A (1972). The nature of the membrane sites controlling anion permeability of human red blood cells as determined by studies with disulfonic stilbene derivatives. *J Membr Biol* **10**, 311–330.

Cass A & Dalmark M (1973). Equilibrium dialysis of ions in nystatin-treated red cells. *Nat New Biol* **244**, 47–49.

Cueff A, Seear R, Dyrda A, Bouyer G, Egee S, Esposito A, Skepper J, Tiffert T, Lew VL & Thomas SL (2010). Effects of elevated intracellular calcium on the osmotic fragility of human red blood cells. *Cell Calcium* **47**, 29–36.

Dalmark M (1975). Chloride and water distribution in human red cells. *J Physiol* **250**, 65–84.

Eisner DA, Kenning NA, O'Neill SC, Pocock G, Richards CD & Valdeolmillos M (1989). A novel method for absolute calibration of intracellular pH indicators. *Pflugers Arch* **413**, 553–558.

Ellis D & Thomas RC (1976). Microelectrode measurement of the intracellular pH of mammalian heart cells. *Nature* **262**, 224–225.

Escobales N & Canessa M (1986). Amiloride-sensitive Na^+ transport in human red cells: evidence for a Na/H exchange system. *J Membr Biol* **90**, 21–28.

Freeman CJ, Bookchin RM, Ortiz OE & Lew VL (1987). K-permeabilized human red cells lose an alkaline, hypertonic fluid containing excess K over diffusible anions. *J Membr Biol* **96**, 235–241.

Funder J & Wieth JO (1966). Chloride and hydrogen ion distribution between human red cells and plasma. *Acta Physiol Scand* **68**, 234–245.

Funder J & Wieth JO (1976). Chloride transport in human erythrocytes and ghosts: a quantitative comparison. *J Physiol* **262**, 679–698.

Garcia-Sancho J (1985). Pyruvate prevents the ATP depletion caused by formaldehyde or calcium-chelator esters in the human red cell. *Biochim Biophys Acta* **813**, 148–150.

Garcia-Sancho J & Lew VL (1988). Detection and separation of human red cells with different calcium contents following uniform calcium permeabilization. *J Physiol* **407**, 505–522.

Gardos G (1958). The function of calcium in the potassium permeability of human erythrocytes. *Biochim Biophys Acta* **30**, 653–654.

Gatto C & Milanick MA (1993). Inhibition of the red blood cell calcium pump by eosin and other fluorescein analogues. *Am J Physiol Cell Physiol* **264**, C1577–1586.

Grynkiewicz G, Poenie M & Tsien RY (1985). A new generation of Ca^{2+} indicators with greatly improved fluorescence properties. *J Biol Chem* **260**, 3440–3450.

Humphreys BD, Jiang L, Chernova MN & Alper SL (1994). Functional characterization and regulation by pH of murine AE2 anion exchanger expressed in *Xenopus* oocytes. *Am J Physiol Cell Physiol* **267**, C1295–1307.

Jacobs MH & Stewart DR (1947). Osmotic properties of the erythrocyte; ionic and osmotic equilibria with a complex external solution. *J Cell Physiol* **30**, 79–103.

Kaestner L, Tabellion W, Weiss E, Bernhardt I & Lipp P (2006). Calcium imaging of individual erythrocytes: problems and approaches. *Cell Calcium* **39**, 13–19.

Kaplan JH, Pring M & Passow H (1983). Band-3 protein-mediated anion conductance of the red cell membrane. Slippage vs ionic diffusion. *FEBS Lett* **156**, 175–179.

Knauf F, Yang CL, Thomson RB, Mentone SA, Giebisch G & Aronson PS (2001). Identification of a chloride–formate exchanger expressed on the brush border membrane of renal proximal tubule cells. *Proc Natl Acad Sci U S A* **98**, 9425–9430.

Knauf PA, Law FY, Leung TW, Gehret AU & Perez ML (2002). Substrate-dependent reversal of anion transport site orientation in the human red blood cell anion-exchange protein, AE1. *Proc Natl Acad Sci U S A* **99**, 10861–10864.

Knauf PA, Law FY & Marchant PJ (1983). Relationship of net chloride flow across the human erythrocyte membrane to the anion exchange mechanism. *J Gen Physiol* **81**, 95–126.

Koren W, Grienspuhn A, Kuznetsov SR, Berezin M, Rosenthal T & Postnov YV (1998). Enhanced Na^+/H^+ exchange in Cushing's syndrome reflects functional hypermineralocorticoidism. *J Hypertens* **16**, 1187–1191.

Kummerow D, Hamann J, Browning JA, Wilkins R, Ellory JC & Bernhardt I (2000). Variations of intracellular pH in human erythrocytes via $K^+(Na^+)/H^+$ exchange under low ionic strength conditions. *J Membr Biol* **176**, 207–216.

Lee BS, Gunn RB & Kopito RR (1991). Functional differences among nonerythroid anion exchangers expressed in a transfected human cell line. *J Biol Chem* **266**, 11448–11454.

Leem CH, Lagadic-Gossmann D & Vaughan-Jones RD (1999). Characterization of intracellular pH regulation in the guinea-pig ventricular myocyte. *J Physiol* **517**, 159–180.

Lew VL & Bookchin RM (1986). Volume, pH, and ion-content regulation in human red cells: analysis of transient behavior with an integrated model. *J Membr Biol* **92**, 57–74.

Lew VL & Bookchin RM (2005). Ion transport pathology in the mechanism of sickle cell dehydration. *Physiol Rev* **85**, 179–200.

Lew VL, Daw N, Etzion Z, Tiffert T, Muoma A, Vanagas L & Bookchin RM (2007). Effects of age-dependent membrane transport changes on the homeostasis of senescent human red blood cells. *Blood* **110**, 1334–1342.

Lew VL, Etzion Z, Bookchin RM, daCosta R, Vaananen H, Sassaroli M & Eisinger J (1993). The distribution of intracellular calcium chelator (fura-2) in a population of intact human red cells. *Biochim Biophys Acta* **1148**, 152–156.

Lew VL & Ferreira HG (1978). Calcium transport and the properties of a calcium-activated potassium channel in red cell membranes. In *Current Topics in Membranes and Transport*, ed. Kleinzeller A & Bronner F, pp. 217–277. Academic Press, New York.

Lew VL, Freeman CJ, Ortiz OE & Bookchin RM (1991). A mathematical model of the volume, pH, and ion content regulation in reticulocytes. Application to the pathophysiology of sickle cell dehydration. *J Clin Invest* **87**, 100–112.

Lew VL, Raftos JE, Sorette M, Bookchin RM & Mohandas N (1995). Generation of normal human red cell volume, hemoglobin content, and membrane area distributions by "birth" or regulation? *Blood* **86**, 334–341.

Maren TH (1967). Carbonic anhydrase: chemistry, physiology, and inhibition. *Physiol Rev* **47**, 595–781.

Mason MJ, Smith JD, Garcia-Soto JJ & Grinstein S (1989). Internal pH-sensitive site couples Cl^-–HCO_3^- exchange to Na^+-H^+ antiport in lymphocytes. *Am J Physiol Cell Physiol* **256**, C428–433.

Meldrum NU & Roughton FJ (1933). Carbonic anhydrase. Its preparation and properties. *J Physiol* **80**, 113–142.

Mount DB & Romero MF (2004). The SLC26 gene family of multifunctional anion exchangers. *Pflugers Arch* **447**, 710–721.

Olsnes S, Tonnessen TI & Sandvig K (1986). pH-regulated anion antiport in nucleated mammalian cells. *J Cell Biol* **102**, 967–971.

Papageorgiou P, Shmukler BE, Stuart-Tilley AK, Jiang L & Alper SL (2001). AE anion exchangers in atrial tumor cells. *Am J Physiol Heart Circ Physiol* **280**, H937–945.

Roos A & Boron WF (1981). Intracellular pH. *Physiol Rev* **61**, 296–434.

Salenius P (1957). A study of the pH and buffer capacity of blood, plasma and red blood cells. *Scand J Clin Lab Invest* **9**, 160–167.

Salminen S & Manninen V (1966). Ion and water shifts produced by ammonium chloride in high K and low K red cells. *J Cell Physiol* **68**, 19–24.

Sarangarajan R, Dhabia N, Soleimani M, Baird N & Joiner C (1998). NHE-1 is the sodium-hydrogen exchanger isoform present in erythroid cells. *Biochim Biophys Acta* **1374**, 56–62.

Sterling D & Casey JR (2002). Bicarbonate transport proteins. *Biochem Cell Biol* **80**, 483–497.

Stewart AK, Kerr N, Chernova MN, Alper SL & Vaughan-Jones RD (2004). Acute pH-dependent regulation of AE2-mediated anion exchange involves discrete local surfaces of the NH2-terminal cytoplasmic domain. *J Biol Chem* **279**, 52664–52676.

Strobaek D, Teuber L, Jorgensen TD, Ahring PK, Kjaer K, Hansen RS, Olesen SP, Christophersen P & Skaaning-Jensen B (2004). Activation of human IK and SK Ca^{2+}-activated K^+ channels by NS309 (6,7-dichloro-1H-indole-2,3-dione 3-oxime). *Biochim Biophys Acta* **1665**, 1–5.

Sun B, Leem CH & Vaughan-Jones RD (1996). Novel chloride-dependent acid loader in the guinea-pig ventricular myocyte: part of a dual acid-loading mechanism. *J Physiol* **495**, 65–82.

Thomas JA, Buchsbaum RN, Zimniak A & Racker E (1979). Intracellular pH measurements in Ehrlich ascites tumor cells utilizing spectroscopic probes generated in situ. *Biochemistry* **18**, 2210–2218.

Tiffert T, Daw N, Etzion Z, Bookchin RM & Lew VL (2007). Age decline in the activity of the Ca^{2+}-sensitive K^+ channel of human red blood cells. *J Gen Physiol* **129**, 429–436.

Tiffert T, Etzion Z, Bookchin RM & Lew VL (1993). Effects of deoxygenation on active and passive Ca^{2+} transport and cytoplasmic Ca^{2+} buffering in normal human red cells. *J Physiol* **464**, 529–544.

Tiffert T, Garcia-Sancho J & Lew VL (1984). Irreversible ATP depletion caused by low concentrations of formaldehyde and of calcium-chelator esters in intact human red cells. *Biochim Biophys Acta* **773**, 143–156.

Van Slyke DD, Wu H & McLean FC (1923). Studies of gas and electrolyte equilibria in the blood. V. Factors controlling the electrolyte and water distribution in the blood. *J Biol Chem* **56**, 765–849.

Vandorpe DH, Shmukler BE, Jiang L, Lim B, Maylie J, Adelman JP, de Franceschi L, Cappellini MD, Brugnara C & Alper SL (1998). cDNA cloning and functional characterization of the mouse Ca^{2+}-gated K^+ channel, mIK1. Roles in regulatory volume decrease and erythroid differentiation. *J Biol Chem* **273**, 21542–21553.

Vaughan-Jones RD (1982). Chloride activity and its control in skeletal and cardiac muscle. *Philos Trans R Soc Lond B Biol Sci* **299**, 537–548.

Vaughan-Jones RD, Spitzer KW & Swietach P (2009). Intracellular pH regulation in heart. *J Mol Cell Cardiol* **46**, 318–331.

Zhang Y, Chernova MN, Stuart-Tilley AK, Jiang L & Alper SL (1996). The cytoplasmic and transmembrane domains of AE2 both contribute to regulation of anion exchange by pH. *J Biol Chem* **271**, 5741–5749.

Author contributions

P.S., T.T., V.L.L. & R.D.V-J.: Conceived and designed project; confocal imaging and cell cytometry performed in DPAG, Oxford with sample preparation in DPDN, Cambridge. Data analysis and manuscript writing in DPAG, Oxford and DPDN, Cambridge. J.M.A.M., R.S., E.P., C.F.K.: additional exploratory

experiments (confocal imaging) in DCEB, Cambridge. All authors have approved the final version for publication.

Acknowledgements

This work was supported by grants from the British Heart Foundation (RG/08/016/26423, to R.D.V.-J.), the Royal Society (a University Research Fellowship to P.S.), the MRC (G0700698; to P.S.), the BBSRC (BB/E008542/1 to C.F.K., T.T. and V.L.L.), the EPSRC (EP/E059384 to C.F.K., T.T., V.L.L. and J.M.A.M., and EP/FO44011/1 to A.E.), and the Isaac Newton Trust (to T.T.).